

**Theoretical Modelling of
the Temperature Distribution
in
Laser-induced
Hyperthermia**

Diploma Paper
Christian Sturesson

Lund Reports on Atomic Physics, LRAP-159
Lund, April 1994

Abstract

Hyperthermia can be used for tumour treatments. It implies the heating of cells with a following cell death. Classically, the temperature used in hyperthermia treatment ranges between 41-46 °C. This is due to an observed greater heat sensibility of tumour tissue compared to healthy tissue at these temperatures. In all hyperthermia treatments it is of vital importance to know the tissue temperature. This is usually accomplished by inserting temperature probes into the tissue, but can also be calculated by a model for the heating and the heat transport in tissue. This work discusses laser-induced hyperthermia. A computer model for calculating the temperature distribution in a laser irradiated tissue was constructed. The validity of the model was examined by comparing its predictions with experimental data obtained for a beef liver.

Acknowledgements

I would like to thank Dr. Stefan Andersson-Engels who outlined this project and helped me throughout my work.

I would also like to thank Dr. Göran Hellström at the Department of Mathematical Physics, Lund Institute of Technology, for kindly providing me with the basic numerical algorithms for the numerical heat transfer model.

Finally, I would like to thank Professor Sune Svanberg and the numerous people at the Division of Atomic Physics not mentioned by name who made this work possible.

Table of Contents

Abstract	i
Acknowledgements	ii
1. Introduction	3
2. Cancer	4
2.1 Description of Cancer	4
3. The Liver	4
3.1 Morphology of the Liver	4
3.2 Liver Cancer Treatment	6
4. Heat Treatment of Cancer	7
4.1 The Impact of Heat to Cells	7
5. Techniques for Hyperthermia Treatment	8
6. Tissue Optics	9
6.1 Light-tissue Interaction	9
7. Monte Carlo Simulation	10
7.1 Photon Propagation	10
7.2 Photon Absorption	12
7.3 Photon Scattering	12
7.4 Reflection or Transmission at Boundaries and Interfaces	13
7.5 Photon Termination	13
7.6 Finite Beam Size	13
8. Thermal Diffusion	14
8.1 Mathematical Model	14
8.2 Numerical Solution	15
8.2.1 The Numerical Method	16
8.2.2 Boundary Conditions	18
8.2.3 Method Stability	18
8.3 Solution Validity	19
8.3.1 Axial Conductance	19
8.3.2 Radial Conductance	20
8.3.3 Line Source	22
8.3.4 Grid Size	23
9. Experimental Method	26
9.1 Experimental Set-up	26
9.2 Thermistor Calibration	26
10. Model Coefficients	27

11 Results	28
11.1 Nd:YAG Laser Results	28
11.2 Argon Ion Laser Results	32
12 Discussion and Conclusions	33
12.1 Result Interpretation	33
12.2 Measurement Uncertainties	34
12.3 The Influence of Charring	34
12.4 Future Prospects	35
13 List of References	36
14 Appendices	38
A Heat Transfer Source Code	38
B Temperature Conversion Source Code	45

1 Introduction

In the treatment of tumours, a number of different treatment modalities has been developed. Among these are surgical resection, radiotherapy, chemotherapy and photodynamic therapy (PDT) [1,2]. The clinician's choice of therapeutic method depends on the tumour type and location. In many cases, a combination of treatment modalities is to be preferred. Despite the large arsenal of treatment modalities, some tumours are still resistant to these treatments. Thus, new and refined therapeutic methods are under development, such as various hyperthermia techniques.

Hyperthermia signifies the induction of a temperature rise in cells above body temperature. As the cells are temperature-sensitive, specific heating of tumour cells can incite their death.

The use of hyperthermia in tumour treatment is far from new. The first medical text mentioning hyperthermia is an Egyptian papyrus dated more than 5000 years back. However, after a long time in obscurity, hyperthermia as a tumour treatment modality has in the recent years gained a renewed interest among clinicians and researchers.

Clinically, hyperthermia is today frequently combined with other therapeutic methods in order to attain an additive or synergistic effect. In the majority of these treatments, the combination of radiotherapy - hyperthermia has been utilised. The results show, however not conclusively, greater and longer-lasting tumour regression with irradiation combined with hyperthermia than with irradiation alone [3]. Similar results has also been reported for the combination of hyperthermia and chemotherapeutic drugs [4].

In conjunction with PDT, there has also been reported synergistic effects when applying hyperthermia after PDT treatment [5-7]. The therapeutic depth of PDT is only a few millimetres so PDT combined with hyperthermia can be used to induce lesions of greater depth than is possible with PDT alone.

Hyperthermia treatments rely on the knowledge of the tissue temperature. The temperature and the time of heating, called the thermal dose or thermal history, determine the tissue damage. Today, the tissue temperature is usually measured by temperature probes inserted into the tumour treated.

The concept of thermal dose is still unsatisfactorily developed. Obviously, the number of probes that can be inserted into a tumour is limited. This gives information about the temperature at a few points only. Being able to predict the temperature distribution within the tissue would give an attractive method of temperature control and a tool for determining the dose needed to achieve the desired result. This project is an attempt to mathematically model the hyperthermia process in tissues; more specifically in the liver.

The present work treats the progressive method of laser-induced hyperthermia. Laser light has the advantage of heating a spatially well defined region. Also, the amount of energy delivered to the tissue can be precisely determined using laser heating and the possibility of coupling the laser light through thin optical fibres for interstitial treatment makes the method convenient.

In this report, the concept of cancer and the liver morphology are briefly presented, followed by a description of the cell damages occurring on heating.

The model made for tissue heating includes laser light absorption and the subsequent heat propagation. These events and the chosen numerical solutions to the problems are presented.

Finally, the agreement between the model-calculated temperature distributions and experimental results is investigated.

2 Cancer

The healthy human body depend on the co-operative and self-sacrificing behaviour of its cells. All the body cells, somatic cells, are destined to die, dedicating their existence to support the germ cells which alone have a chance of survival. In this way, the somatic cells help their own future existence as the genome, the set of genes, are the same for the germ and somatic cells.

In contrast with free-living cells such as bacteria which compete to survive, the cells of a multicellular organism are committed to collaboration. This collaborative manner can be disturbed if individual cells begin to proliferate selfishly. Cancer is such a disturbance with the death of the whole cellular society in the end.

2.1 Description of Cancer

Cancer cells are defined by two properties that distinguish them from normal cells. Firstly, they reproduce neglecting the normal cell-dividing signals, and secondly, they invade and colonise territory normally reserved for other cells.

Abnormal cells proliferating faster than the surrounding cells will give rise to a tumour, or neoplasm. If the abnormal cells are incapable of escaping the tumour, the tumour is said to be benign. If the cells are able to emigrate and found new colonies, metastases, elsewhere in the body, the tumour is called malignant. A tumour is counted as a cancer only if it is malignant.

Most cancers can be traced to have evolved from a primary tumour, suggesting that a single cell insurrection to the cell-dividing control mechanism is the cause for the disease. Tumours are dependent on blood supply to get oxygen and nutrients. The growth of a solid tumour is made possible by the invasion of capillaries. It is thought that tissues, normal as well as tumour, deprived of oxygen, release factors that induce capillary growth.

3 The Liver

The liver is the largest gland in the human body, comprising approximately 2.5 % of the total body weight. It is the main site where nutrients, absorbed from the gut and then transferred to the blood, are processed for the use by other cells in the body. Foreign substances are filtered by the liver and it handles the products of heme metabolism. The liver secretes bile, an emulsifying agent helping the absorption of fats. It further participates in the regulation of blood volume and blood flow. The liver is also an efficient source of phagocytosis of materials such as bacteria.

3.1 Morphology of the Liver

The most prominent cell in the liver is the hepatocyte. The hepatocytes account for 80 % of the liver volume. They are arranged in folded sheets, facing the blood filled spaces called sinusoids (Fig. 3.1).

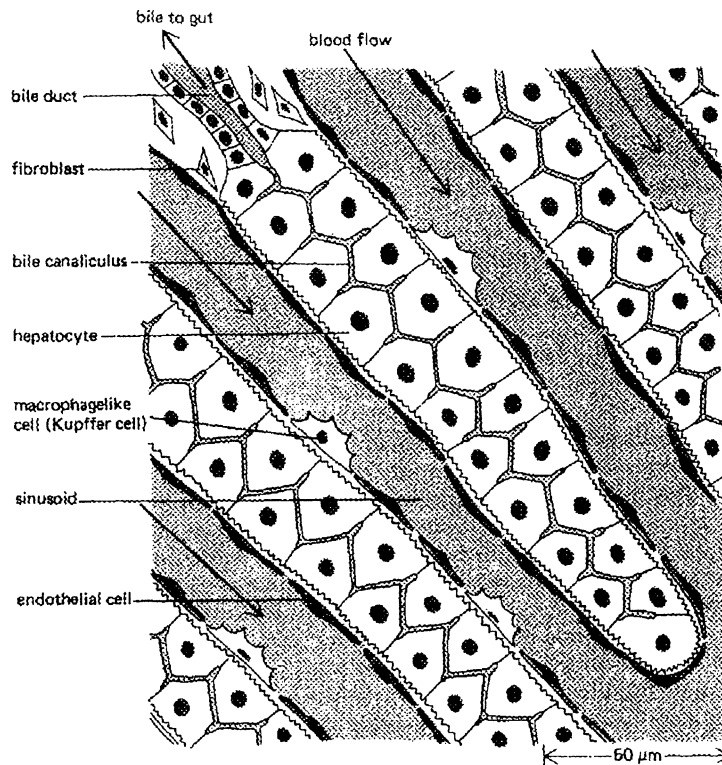


Fig. 3.1. Illustration of the different liver cells (from Ref. 8).

The hepatocytes are separated from the blood flow by a single thin sheet of endothelial cells protecting the hepatocytes from direct contact with the blood. Macrophage-like Kupffer cells are interposed between the endothelial cells. The Kupffer cells engulf bacteria and worn-out red blood cells.

Centrally located between adjacent hepatocytes are the bile canaliculi, minute bile channels. Via bile ducts, biliary products are delivered from the liver to the common bile duct and eventually to the small intestine.

A small number of fibroblasts provide a supporting framework of connective tissue.

Two major vessels supply blood to the liver. 75 % of the blood supply comes from the portal vein. This blood is rich in nutrients. The remaining 25 % is carried by the hepatic artery, containing the majority of the oxygen needed for the survival of the liver.

The liver can be divided into two physiological halves, the right and the left lobe, by the branching point of the portal vein, hepatic artery and bile duct (Fig. 3.2).

The entire external surface of the liver is covered by a thin capsule of connective tissue mainly made up by collagen. The capsule is continuous with the connective tissue inside the liver.

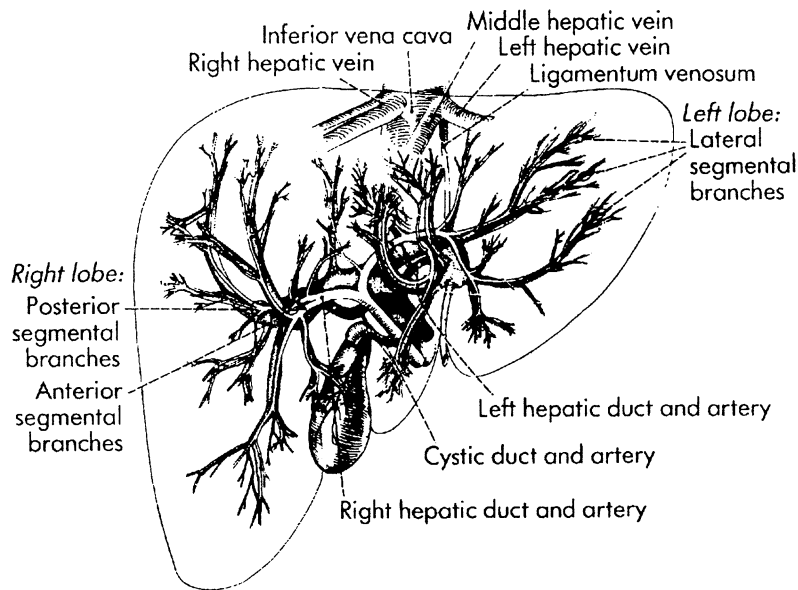


Fig. 3.2. Schematic picture of the liver and its main vessels (from Ref. 9).

3.2 Liver Cancer Treatment

In the Western world, metastases from other organs represent the most common neoplasm in the liver. Metastases are most common from a primary tumour in breast, lung, pancreas or colon, stated in order of significance. Over 50 % of the patients with colorectal cancer will develop liver metastases. Patients with secondary liver tumours have a poor prognosis. Survival for more than one year after detection is rare [10].

The vascular nature of the liver poses problems with excessive bleeding at the time of resection, imposing the need of treatment methods reducing the blood loss.

Treatment options of liver tumours is limited, only a small percentage is suitable to undergo surgical resection [11]. This is due to the problems of blood loss and the fact that resection of the tumours entail gross normal liver tissue removal. The surgical procedure can thus be so severe for the liver that it fails to uphold its function.

Some alternative methods are chemotherapy, radiotherapy, cryotherapy, alcohol injection and interstitial hyperthermia.

Chemotherapy. Antitumour agents can either be distributed in the whole body or regionally in the disease-bearing region. Liver tumours have, however, generally been found to be only moderately sensitive to single chemotherapeutic drugs [9].

Radiotherapy. Normal liver tissue has a limited tolerance to radiation. Radiation therapy is therefore mostly combined with other therapeutic methods. Radioactive sources can be implanted in the tumour tissue for site-directed delivery of high intensity radiation which would not be feasible with external beam techniques.

Cryotherapy. Nitrogen-cooled probes can be used to freeze tumours. The method has the disadvantage of requiring operation in order to place the comparatively large probes in or near the tumours. Thereby, the morbidity is enhanced due to the surgical procedure.

Alcohol injection. Ethanol can be injected through fine needles into the tumours during ultrasonic guidance. A problem is the unpredictable geometrical alcohol distribution occurring after injection, and the following imprecise area of necrosis [10].

4 Heat Treatment of Cancer

Hyperthermia, or the use of heat for medical purposes, has a long and excessive history which can be traced back to antiquity. It is known that a temperature rise even by a few degrees will cause cell injuries. The severity of the lesions is dependent on the temperature level and the time of the increased temperature. These two factors are called the thermal history [12]. The thermal history rather than the peak cell temperature is what determines the heat damage. In the struggle against cancer, the desired damage is the severest possible: cell killing.

4.1 The Impact of Heat to Cells

In tumour therapy, a temperature range of 41-46 °C is often utilised [13]. The cell injuries at this temperature are in most cases reversible provided the treatment is interrupted sufficiently soon. When the exposure continues for a longer time, ranging from a few minutes to several hours [13] depending on the type of tissue, an irreversible step is attained leading to cell necrosis. The mechanism of heat-induced cell killing is not fully understood, but assumptions based on observations can be done.

An elevated cell temperature causes conformational changes in macromolecule structures caused by the breaking of van der Waal's forces in the molecules. This effect leads to the inhibition of DNA, RNA and protein synthesis and the breakdown of membranes and the cytoskeleton. These alterations are believed to be very important for cell death [14]. Sharp denaturation transitions may exist for certain enzymes at temperatures only a few degrees above normal body temperature. Proteins denature in the range of 42-65 °C and DNA at about 80-85 °C [15]. However, it is the complete temperature-time history that determines the degree of denaturation.

Hyperthermia also affects the microcirculation and thereby the cells. Tissue and cellular oedema due to thermally induced vascular and cellular membrane injury appears several minutes to several hours after heating [16].

An event known as thermotolerance has been observed during heating for a few hours below 42.5 °C or succeeding a brief heat shock [17]. In this case, the cell starts synthesizing a special set of proteins, called heat shock or stress-response proteins [8]. The heat shock proteins are likely to solubilise and refold denatured and misfolded proteins. Thermotolerance is a transient state of thermal resistance.

It has been found that tumours are more sensitive to heat than normal tissues. In solid tumours it is likely to find a deficit in oxygen, low pH and energy deprivation; factors that render the tumour sensitive to heat. These features depend mostly on the tumour microcirculation, which is generally insufficient in larger tumours [18]. The weak microcirculation also limits the heat dissipation from tumour tissue, which makes it easier to selectively heat tumours and not healthy tissue.

The small difference in heat sensitivity between tumour and normal tissue is lost at 50 °C [12].

Another phenomenon that can occur is the visible whitening of the tissue treated, indicating thermal coagulation. Thermal coagulation is mostly due to denaturation of structural proteins, and is an irreversible process. More correctly this is not *one* process, but a wide range of coagulative changes that seem to occur at different temperatures and heating times [16].

Coagulated cells shrink due to thermal denaturation, the contraction of structural proteins and probably the rupture of the cytoskeleton. Their nuclei and cytoplasm become dense because of the condensation of chromatin and cytoplasm proteins [12].

In more severely damaged cells, an extensive membrane rupture is observed. Membrane fragments form closed or partially closed spheroids and irregular isolated sheets [19]. Coagulation can cause hemostasis if the heat denatures blood proteins which occludes the blood vessels.

When the temperature exceeds 100 °C water begins to vaporise. This induces a complicated process with rapidly expanding steam vacuoles within the tissue. Microexplosions, due to the expanding gas bubbles, can fragmentise the tissue.

Tissue heated beyond the vaporisation of water is ablated and carbonised. This provides a method for the removal of tissue.

5 Techniques for Hyperthermia Treatment

Different techniques inducing hyperthermia can basically be categorised into four methods: electromagnetic techniques, ultrasound, thermal conduction and radiant light [20].

Electromagnetic Techniques. A current can be passed through the tissue between two electrodes, inducing heat by the motion of ions. The method can be either interstitial or non-invasive if the electrodes is placed inside or outside the body, respectively. Usually a frequency below 30 MHz is used.

Another way of inducing heat is to use a radiative method. Antennas can be introduced within the body. Generally a frequency of 25 MHz and above has been used. This technique transmits energy from a single or an array of antennas. The most popular and best heating technique in this group rely on the use of a microwave antenna array, inserted in the tissue as a series of small coaxial antennas.

Ultrasound. Ultrasound methods have a high penetration depth and can cause highly focused heating. Heat patterns generally form a very oblique ellipsoid with the long axis along the depth direction. This technique provides an interesting treatment modality for non-invasive tumour destruction. However, the application is limited in the presence of air and bone.

Thermal Conduction. Superficial tumours can be treated simply by holding a hot surface to the tissue. For substantial heating, this method has an approximate 2 mm depth limit.

Radiant Light. In this category falls the use of lasers for inducing hyperthermia. This subject will be discussed in the following section.

6 Tissue Optics

The effects of laser irradiation of tissues can be separated into three major categories - photochemical, photothermal and photomechanical [21].

Photochemical effects depend on the absorption of the laser light to induce chemical reactions as in photodynamic therapy (PDT).

Photothermal effects follow the transformation of light energy to heat, inducing cell injury or destruction.

Photomechanical effects result when short, high-energy laser pulses produce mechanical forces that disrupts cells and tissues.

The categories are interconnected in a sometimes unknown manner. For instance, as mentioned above, it has been proposed that a synergistic tumour treatment effect occurs when combining PDT and hyperthermia. In the following account, the isolated event of laser hyperthermia will be further developed.

6.1 Light-tissue Interaction

Laser light used to induce tissue hyperthermia ranges from the visible to the infrared range of the electromagnetic spectrum. The light is absorbed by the tissue and converted to heat. In the optical model of tissue, when describing the light as photons, the following events can occur (Fig. 6.1):

- 1) reflection at the surface (not shown in figure)
- 2) retro-diffusion after scattering
- 3) absorption before and after scattering
- 4) direct transmission
- 5) transmission after scattering

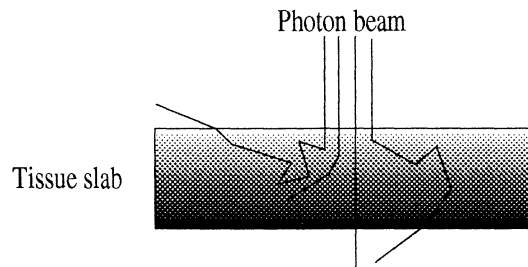


Fig. 6.1. Different possible photon events when entering a tissue slab.

The tissue absorption is characterised by an absorption coefficient, denoted μ_a . Two other factors are often used to characterise the optical properties of tissue, namely the scattering coefficient, μ_s , and a phase function defining an anisotropy factor, g .

The absorption coefficient is in units of cm^{-1} . Its inverted value, $1/\mu_a$, indicates the mean free path of a photon before absorption.

The scattering coefficient is also expressed in units of cm^{-1} . The inverted value gives the mean free path before a photon is scattered. For the wavelengths mentioned above, scattering is much more probable than absorption in tissue.

The phase function P describes the spatial distribution of scattering as a function of $\cos\Theta$, where Θ is the deflection angle (Fig. 6.2). Let $\alpha = \cos\Theta$, then $P(\alpha)d\alpha$ equals the probability that a scattered photon is deflected an angle between Θ and $\Theta + \Delta\Theta$, where $\Delta\Theta$ equals $\sin\Theta d\Theta$.

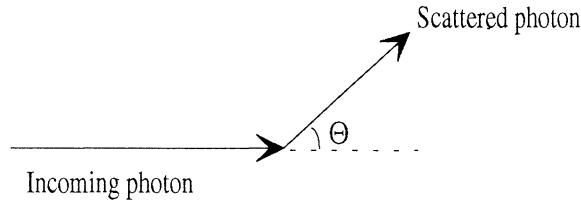


Fig. 6.2. Illustration of the deflection angle Θ .

The name "phase function" has no correlation to the phase of the light, but refers to galactic phases. It was in astronomy this concept first was utilised [22]. The anisotropy, g , equals the expectation value $\langle \cos\Theta \rangle$. A factor g equal to zero indicates isotropic scattering, the light is scattered randomly in all directions. When the anisotropy factor approaches unity, the scattering becomes more and more accentuated in the forward direction. The reverse process is described with a factor g between zero and -1. Many tissues have an anisotropy factor of approximately 0.9, which indicates a modest deflection.

Optical models that exploit these quantities in describing the optical properties of tissue are the transport theory, the transport theory employing the diffusion approximation [22] and Monte Carlo simulation methods. Yet another model, called the Kubelka-Munk, Schuster or two flux theory [23] utilises different characterising coefficients for the tissue. This study is confined to the description and utilisation of the Monte Carlo simulation model.

7 Monte Carlo Simulation

There is no well-established definition of a Monte Carlo method, but they all work with some kind of stochastic model where a physical quantity is determined using multiple independent samples generated randomly under certain conditions.

In a light propagation model, the Monte Carlo simulations consist of launching photons into a medium, and tracing the individual photon histories. In the present work, this is done by the computer program "Monte Carlo Modelling in Multi-layered Tissues in Standard C", 1992, created by L. Wang and S. Jacques.

7.1 Photon Propagation

The method is based on the assumption that photons propagating through tissue can be treated as neutral particles and that wave phenomena can be disregarded.

Ignoring polarisation, inelastic scattering and fluorescence, the model is defined by three quantities:

- 1) the absorption coefficient, μ_a
- 2) the scattering coefficient, μ_s
- 3) the phase function

A photon propagating in a medium has a probability, $p(s)$, that an event (scattering or absorption) occurs after travelling a distance of s cm. This can be expressed as

$$p(s) = \mu_t e^{-\mu_t s} \quad (7.1)$$

where μ_t is the interaction coefficient and equals $\mu_t = \mu_a + \mu_s$.

Integration of (7.1) gives the probability that an event has occurred before the photon has travelled the distance s_1 .

$$P(0 < s \leq s_1) = 1 - e^{-\mu_t s_1} \quad (7.2)$$

Taken a random variable, ξ , uniformly distributed over the interval $[0,1]$, it is assumed that there exists a non-decreasing function $s=f(\xi)$ which maps ξ to s .

This results in

$$P(f(0) < s \leq f(\xi_1)) = P(0 < \xi \leq \xi_1) \quad (7.3)$$

or

$$P(0 < s \leq s_1) = P(0 < \xi \leq \xi_1) \quad (7.4)$$

Comparing this with (7.2) and remembering that ξ has a uniform distribution, it can be concluded that

$$1 - e^{-\mu_t s_1} = \xi_1 \quad (7.5)$$

This leads to

$$s_1 = -\frac{1}{\mu_t} \ln(1 - \xi_1) \quad (7.6)$$

The randomly simulated distance s_1 is the photon step size between photon-tissue interactions.

Equation (7.6) gives the mean free path between photon-tissue interaction,

$$\langle s_1 \rangle = -\frac{1}{\mu_t} \langle \ln(1 - \xi_1) \rangle = \frac{1}{\mu_t} \quad (7.7)$$

as to be expected.

The model allows for defining a grid with arbitrary small grid elements. The grid divides the tissue into boxes where absorbed photons are registered.

Different layers can be defined by characteristic refractive indices (Fig. 7.3).

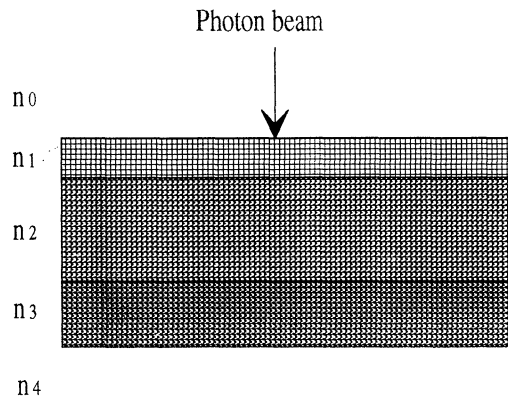


Fig. 7.3. The geometry used in the Monte Carlo simulations.

The model introduces a photon packet with a weight, w , initially assigned a value of one, into the tissue. When a photon packet is launched, some fraction of the weight will be specularly reflected due to mismatch in refractive indices at the boundary surface. The specular reflectance is specified [24] as

$$R_{sp} = \frac{(n_0 - n_1)^2}{(n_0 + n_1)^2} \quad (7.8)$$

where n_0 is the refractive index of the outside medium and n_1 that of the tissue. As a result, the photon weight is decremented:

$$w = 1 - R_{sp} \quad (7.9)$$

7.2 Photon Absorption

After the photon packet has progressed the step size s_1 , the photon weight is decreased by a factor of $w \frac{\mu_a}{\mu_t}$, taking into account the absorption. This factor is stored as absorption in the local grid element. The size of the grid elements is defined before launching. The remaining photon weight is

$$w \left(1 - \frac{\mu_a}{\mu_t} \right) \quad (7.10)$$

This fraction is now scattered.

7.3 Photon Scattering

To simulate a scattering event, it is needed to generate a deflection angle $\theta \in [0, \pi)$ and an azimuth angle $\psi \in [0, 2\pi)$. The azimuth angle is uniformly distributed between 0 and 2π . In order to get a deflection angle, a probability function, or phase function is used. It has been found that the phase function proposed by Heney and Greenstein, originally utilised to describe galactic scattering, is a good approximation to scattering in tissue [25]. This probability function for the cosine of the deflection angle, $\cos\theta$, is expressed as

$$p(\cos\theta) = \frac{1 - g^2}{2(1 + g^2 - 2g\cos\theta)^{1/2}} \quad (7.11)$$

where g is the anisotropy.

Using the same reasoning that lead to (7.5), $\cos\theta$ can be expressed as a function of ξ , the random variable with uniform distribution.

$$\cos\theta = \begin{cases} \frac{1}{2g} \left\{ 1 + g^2 - \left[\frac{1 - g^2}{1 - g + 2g\xi} \right]^2 \right\} & \text{if } g \neq 0 \\ 2g - 1 & \text{if } g = 0 \end{cases} \quad (7.12)$$

The new direction of the photon packet can now be calculated. Subsequently, a new step size s_1 is generated, and the procedure of absorption and scattering is iterated.

7.4 Reflection or Transmission at Boundaries and Interfaces

When reaching a boundary or interface, a photon packet can be totally internally reflected or partially reflected and partially transmitted. Snell's law gives a relationship between the angle of incidence α_i , the angle of transmission α_t , the refractive indices of the medium that the photon is incident from n_i , and transmitted to n_t as

$$n_i \sin \alpha_i = n_t \sin \alpha_t \quad (7.13)$$

An imaginary α_t results in total internal reflectance and the photon packet bounces at the boundary.

In case of a real α_t , the internal reflectance $R(\alpha_i)$ is given as the average of the reflectance for the two orthogonal polarisation directions derived from Fresnel's formulae [24]

$$R(\alpha_i) = \frac{1}{2} \left[\frac{\sin^2(\alpha_i - \alpha_t)}{\sin^2(\alpha_i + \alpha_t)} + \frac{\tan^2(\alpha_i - \alpha_t)}{\tan^2(\alpha_i + \alpha_t)} \right] \quad (7.14)$$

The random variable ξ determines whether the photon packet is transmitted or reflected.

If $\xi \leq R(\alpha_i)$ the photon packet is internally reflected.

If $\xi > R(\alpha_i)$ the photon packet is transmitted.

7.5 Photon Termination

In transmission or reflection out of the medium, the photon tracing terminates. A photon packet propagating in the tissue is submitted to a special procedure when its weight falls below a threshold value. The random variable ξ determines whether the photon tracing should terminate or not.

If $\xi > 1/10$, the photon weight is reduced to zero; the photon is terminated. However, if $\xi \leq 1/10$, the photon weight is multiplied by ten, and the photon tracing continues since the weight now exceeds the threshold value. This procedure, called roulette, ensures energy conservation.

7.6 Finite Beam Size

The simulation is done by launching photon packets from an infinitely narrow beam. To get the responses to a beam with finite size, the launching point can be moved horizontally and more simulations can be done. Alternatively, a convolution of the primary result can be performed.

The first alternative is much too time consuming. Since the problem is linear and invariant, the second option is to prefer.

The linearity means that if the photon packet weight is multiplied by a factor, all the results will be multiplied by the same factor. It also means that the result of two beams applied at the same time, equals the result sum of the two beams taken separately.

The invariance implies that when moving a beam horizontally, the result distribution will be equally displaced.

If the photon beam of finite size is assumed collimated, the response to an infinitely narrow beam will be a Green's function of the tissue system, and the response to a beam of finite size can be calculated from the convolution of the Green's function according to the profile of the finite size photon beam. The simulation program has such a convolution facility, with the two options of flat or Gaussian beam profile.

8 Thermal Diffusion

Once the laser light has been absorbed in the tissue and transformed into heat, the subsequent process is described by the general laws of heat transfer. The thermal diffusion in tissues is basically governed by three different mechanisms: heat conduction, the ability to store heat and the heat dissipation through the vascular system [26].

Heat conduction is based on the effect that heat flows from the warmer regions to the cooler. The heat flux is proportional to the temperature difference per unit length. The proportional constant is called the heat conductivity, λ (W/m K). There is a temperature dependence in the heat conductivity, but if the temperature range is limited this dependence can be neglected [27].

The ability to store heat is expressed by the specific heat capacity, c (J/kg K), which is defined as the ratio of the amount of heat stored to the temperature rise and unit mass of the substance.

The dynamic thermal behaviour of a medium is characterised by the ratio of the thermal conduction properties to the heat storage abilities, called thermal diffusivity, $a=\lambda/\rho c$ (W m²/J). Here, ρ (kg/m³) is the density of the medium.

A basic assumption done from this point is that the thermal properties can be represented by constant values.

In the model made for the temperature distribution, the influence of blood perfusion is disregarded. It has been reported that the obtained temperatures estimated with and without regarding the blood perfusion may be only a few degrees [28]. In the treatment of the liver this simplification can be further justified by the possibility of cutting off the blood supply during surgery.

8.1 Mathematical Model

The processes described above can be expressed mathematically. Fourier's law states that the heat flow \vec{q} at a given point is proportional to the gradient of the temperature

$$\vec{q} = -\lambda \nabla T \quad (8.1)$$

where λ is the thermal conductivity (W/m K).

Consider a volume V in a medium (Fig. 8.1). An energy balance gives

$$\begin{aligned} &\{\text{net energy flowing into the volume}\} + \\ &\{\text{energy production within } V\} = \\ &\{\text{energy storage in } V\} \end{aligned} \quad (8.2)$$

or, in mathematical terms

$$-\int_{\partial V} \vec{q} \cdot \hat{n} \, dA + \int_V A(\vec{r}, t) \, dv = \int_V \rho c \frac{\partial T(\vec{r}, t)}{\partial t} \, dv \quad (8.3)$$

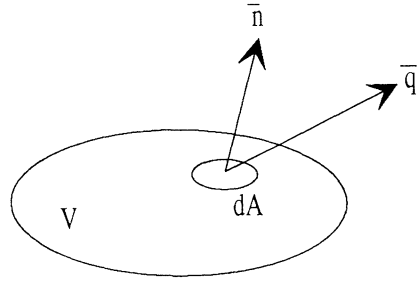


Fig. 8.1. Volume element for energy balance calculation

The term $A(\vec{r}, t)$ is the heat supplied per unit volume per unit time ($\text{J}/\text{m}^3 \text{ s}$) at a point \vec{r} . In the energy storage term, ρ is the density (kg/m^3) and c is the specific heat capacity ($\text{J}/\text{kg K}$).

Using the divergence theorem on the first term of (8.3) yields

$$\int_V (-\nabla \cdot \vec{q} + A(\vec{r}, t) - \rho c \frac{\partial T(\vec{r}, t)}{\partial t}) dV = 0 \quad (8.4)$$

The volume can be chosen arbitrarily small, allowing to remove the integral.

$$-\nabla \cdot \vec{q}(\vec{r}, t) + A(\vec{r}, t) - \rho c \frac{\partial T(\vec{r}, t)}{\partial t} = 0 \quad (8.5)$$

Using (8.1) in (8.5) gives the differential equation of heat conduction

$$\nabla[\lambda \nabla T(\vec{r}, t)] + A(\vec{r}, t) = \rho c \frac{\partial T(\vec{r}, t)}{\partial t} \quad (8.6)$$

When the thermal conductivity is assumed constant, equation (8.6) simplifies to

$$\nabla^2 T(\vec{r}, t) + \frac{1}{\lambda} A(\vec{r}, t) = \frac{1}{a} \frac{\partial T(\vec{r}, t)}{\partial t} \quad (8.7)$$

where $a = \lambda / \rho c$ is the thermal diffusivity. The physical significance is that the higher the thermal diffusivity, the faster is the propagation of heat in the medium.

In the problem treated, the tissue is regarded as a homogenous, isotropic and semi-infinite solid. There is thus only one surface demanding boundary specifications. The boundary condition is chosen to include heat dissipation both through conduction and convection (c.f. 8.2).

8.2 Numerical Solution

The equation of heat conduction (8.7) has been solved numerically. A short description of the numerical method used is presented below. The complete source code to the computer program written in Borland C is found in Appendix A.

8.2.1 The Numerical Method

The tissue-model is divided into grid elements. In each element, the temperature is calculated from a heat flow balance with a time interval of Δt . During this time, steady state heat flow is assumed.

The problem is solved in cylindrical coordinates. Symmetry confines the problem to be two-dimensional (r- and z-direction).

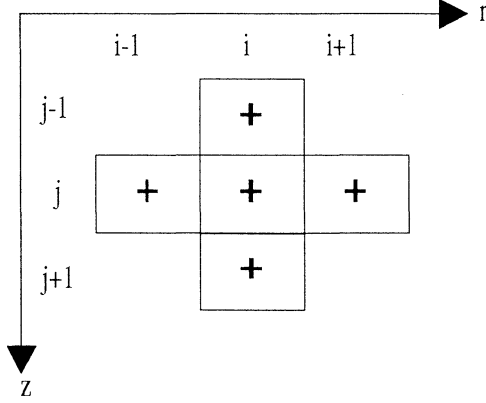


Fig. 8.2. The grid division. In the r-direction, the distance between two middle marks is denoted Δr . The corresponding distance in the z-direction is denoted Δz .

Consider a point at (i, j) (Fig. 8.2). Assuming steady-state heat flow, the heat flux in the z-direction between point (i, j) and point $(i, j+1)$ will be

$$q_z = -\lambda \frac{T_{i,j+1} - T_{i,j}}{\Delta z} \quad (8.8)$$

where Δz is the axial distance between the points.

In the radial direction, using Fourier's law, the steady state heat flow through a circle is

$$Q_r = -2\pi r \lambda \frac{\partial T}{\partial r} \quad (8.9)$$

As the heat flow is independent of r, equation (8.8) is solved by separation of variables

$$Q_r \frac{\partial r}{r} = -2\pi \lambda \partial T \quad (8.10)$$

Integration of (8.10) between circles situated a distance r_i and r_{i+1} from the origin gives

$$Q_r \ln(r_{i+1} / r_i) = -2\pi \lambda (T_{i+1,j} - T_{i,j}) \quad (8.11)$$

or

$$Q_r = \frac{-2\pi \lambda (T_{i+1,j} - T_{i,j})}{\ln(r_{i+1} / r_i)} \quad (8.12)$$

The situation can also be described by means of thermal resistance (Fig. 8.3). By illusively replacing the material of each grid element with a perfect conductor, the elements can be

elements can be imagined being interconnected by thermal resistances. The elements are assigned the temperature $T_{i,j}$, regarded as some kind of average temperature for the cell. With the notation of thermal resistance, assuming steady state heat flow between elements, the axial heat flux between element i,j and element $i,j+1$ and the radial heat flux between element i,j and element $i+1,j$ is

$$q_z = -\frac{1}{R_z}(T_{i,j+1} - T_{i,j}) \quad (8.13a)$$

$$Q_r = -\frac{1}{R_r}(T_{i+1,j} - T_{i,j}) \quad (8.13b)$$

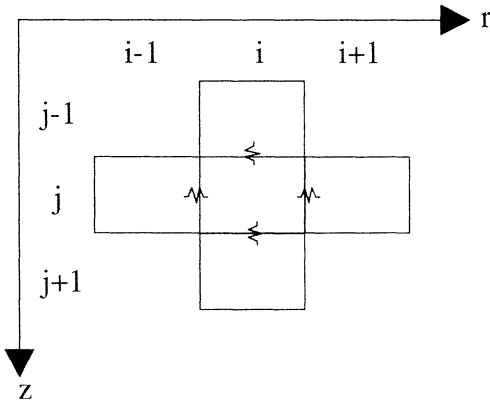


Fig. 8.3. The grid elements as perfect conductors interacting via thermal resistances.

Comparing (8.8) to (8.13a) and (8.12) to (8.13b), the thermal resistances can be identified as

$$\frac{1}{R_z} = \frac{\lambda}{\Delta z} \quad (8.14a)$$

$$\frac{1}{R_r} = \frac{2\pi\lambda}{\ln(r_{i+1}/r_i)} \quad (8.14b)$$

Considering the symmetry, the power flow from element i,j to element $i,j+1$ becomes

$$\Delta P_z = -\frac{1}{R_z}(T_{i,j+1} - T_{i,j}) \times \pi((r_i + \Delta r/2)^2 - (r_i - \Delta r/2)^2) \quad (8.15)$$

The power flow from element i,j to element $i+1,j$ is found in the same way to be

$$\Delta P_r = -\frac{1}{R_r}(T_{i+1,j} - T_{i,j}) \times \Delta z \quad (8.16)$$

Calculating the power flow from all four neighbours and including the source terms gives the temperature rise after a time period of Δt as

$$\Delta T = \frac{(\text{total power flow} + \text{power source} \times \text{element volume}) \times \Delta t}{\rho c \times \text{element volume}} \quad (8.17)$$

This procedure is carried out for all elements before the temperature is updated and the time is incremented by Δt .

The power source is calculated from Monte Carlo simulations and gives the power density as a function of (i,j) .

The temperature calculated should be regarded as the temperature in the middle of each cell, the temperatures of the intermediate regions are given after interpolations.

8.2.2 Boundary Conditions

The temperature of the environment is assumed constant. Heat dissipation through conduction is modelled as above with a thermal resistance (Fig. 8.4) as

$$q_z = -\frac{1}{R_z/2}(T_{i,1} - T_s) \quad (8.18)$$

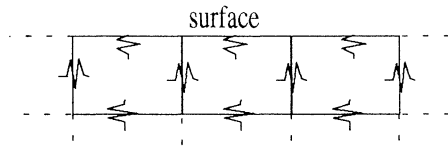


Fig. 8.4. Model of grid elements facing the surface.

Convection is modelled by an additional surface resistance, following Newton's law of cooling, leading to the following expression for the upper boundary

$$q_z = -\frac{1}{R_s + R_z/2}(T_{i,1} - T_s) \quad (8.19)$$

where T_s is the surface temperature.

8.2.3 Method Stability

Stability implicates that uncontrolled temperature oscillations are prevented. The size of the time step is the crucial factor regarding the stability of the method. During the time Δt , the assumed steady-state heat flow must be restricted not to exceed the limitations set by the total energy content in a cell.

This can be formulated as

$$\left(\frac{1}{R_z} (T_{i,j} - T_{i,j-1}) + \frac{1}{R_z} (T_{i,j+1} - T_{i,j}) + \frac{1}{R_{r-1}} (T_{i,j} - T_{i-1,j}) + \frac{1}{R_r} (T_{i+1,j} - T_{i,j}) \right) \Delta t < \quad (8.20)$$

$$\rho c \times \text{vol}_{i,j} \times T_{i,j} + \text{power source}_{i,j} \times \text{vol}_{i,j} \times \Delta t$$

where $\text{vol}_{i,j}$ is the volume of the grid element.

Consider an outflow in all directions. Using absolute temperatures (deg. K), (8.20) gives, when rearranged,

$$\left[\left(\frac{2}{R_z} + \frac{1}{R_{r_{i-1}}} + \frac{1}{R_{r_i}} \right) \Delta t - \rho c \times \text{vol}_{i,j} \right] T_{i,j} < X \quad (8.21)$$

The term X is under these conditions positive. Stability is obtained when Δt fulfils this condition. An underestimation is done by setting X to zero. The final stability condition yields

$$\Delta t_{\text{stab}} < \frac{\rho c \times \text{vol}_{i,j}}{\left(\frac{2}{R_z} + \frac{1}{R_{r_{i-1}}} + \frac{1}{R_{r_i}} \right)} \quad (8.22)$$

8.3 Solution Validity

The numerical model was tested by comparing the numerical results with analytical solutions for different problems. As will be shown, the agreement between the solutions is very good.

8.3.1 Axial Conductance

The one-dimensional problem of heat conduction along the z-axis was modelled by applying a constant surface temperature. For a medium with the same heat conduction parameters as water, the temperature as a function of depth was calculated. This was done for different times.

The analytical solution is simply derived and states, for a semi-infinite solid with an initial temperature of zero and a surface temperature of one degree Celsius

$$T(z, t) = 1 - \text{erf} \left(\frac{z}{2\sqrt{at}} \right) \quad (8.23)$$

where a is the thermal diffusivity.

The error function, erf, is equal to

$$\text{erf}(x) = \frac{2}{\sqrt{\pi}} \int_0^x e^{-\xi^2} d\xi \quad (8.24)$$

Numerical values of the error function can be found in tables.

In Fig. 8.5a, the analytical solution is plotted for a medium with the same heat transfer properties as water ($a=0.6/4.18E6$, $\lambda=0.6$). The numerical result is shown in Fig. 8.5b

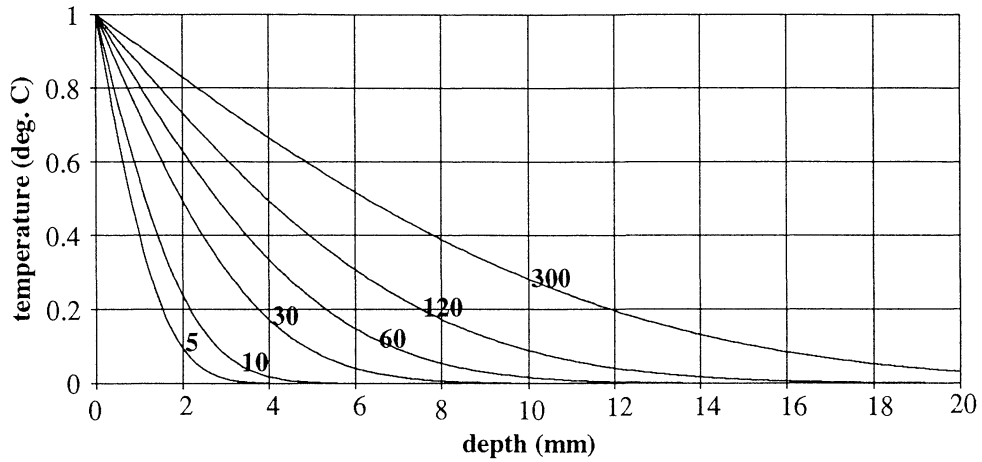


Fig. 8.5a. Axial heat conduction. Analytical solution for a water-like medium. The values on the curves indicate the time.

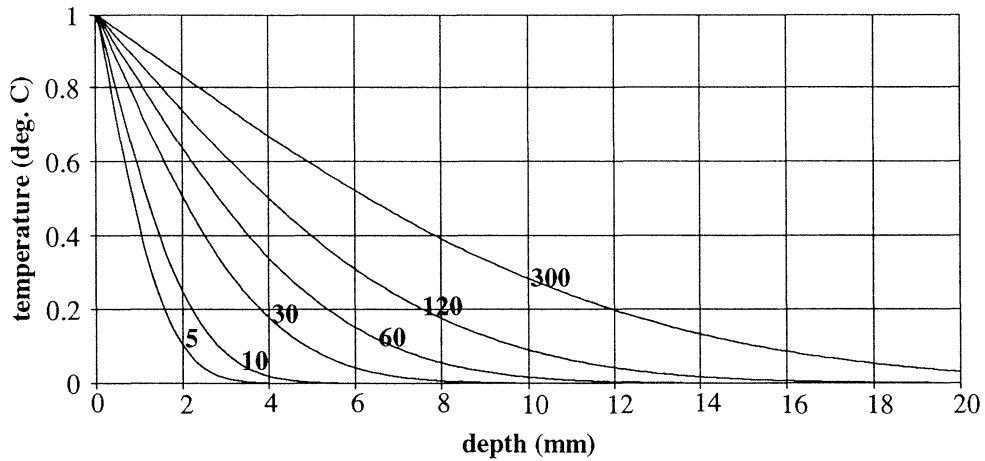


Fig. 8.5b. Numerical calculation of axial heat conduction.

8.3.2 Radial Conductance

The radial heat conduction was tested by applying a constant temperature on the outside of a cylinder in the model. Subsequently, the radial temperature distribution was recorded for different heat conduction constants and times.

The analytical solution is found to be [27]

$$\frac{v}{V} = 1 - 2 \sum_{n=1}^{\infty} e^{-\beta_n^2 at / R^2} \frac{J_0(r\beta_n / R)}{\beta_n J_1(\beta_n)} \quad (8.25)$$

where $\pm\beta_n$ $n=1,2,\dots$ are the roots of $J_0(\beta_n)=0$

J_0 is the Bessel function of the zeroth order of the first kind and J_1 is the Bessel function of the first order of the first kind.

V is the outer surface constant temperature and v is the temperature in the medium. R is the outer radius.

Figs 8.6 a and b shows the numerical and analytical result, respectively.

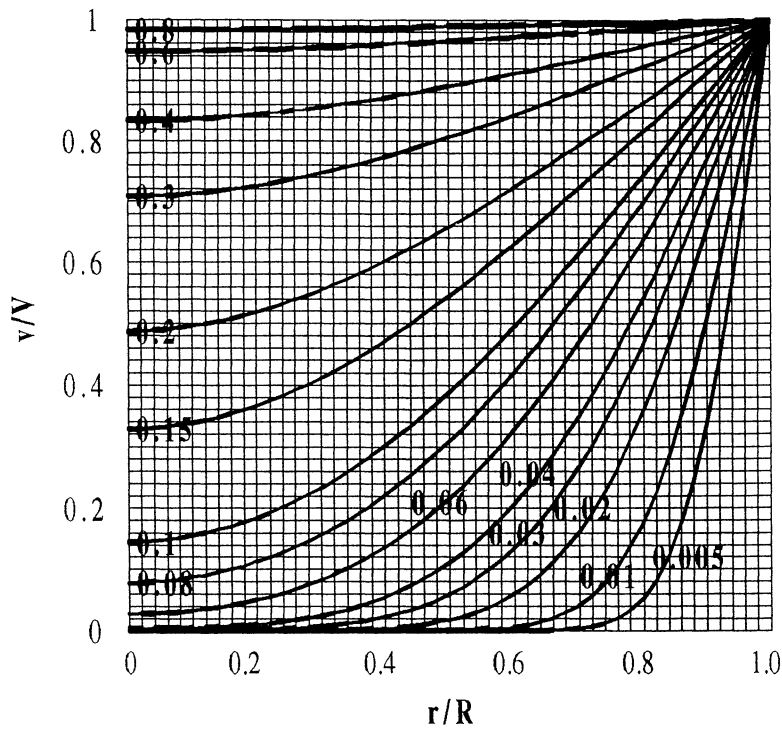


Fig. 8.6a. Radial heat conduction calculated by the numerical model. The numbers on the curves are the values of at/R^2 .

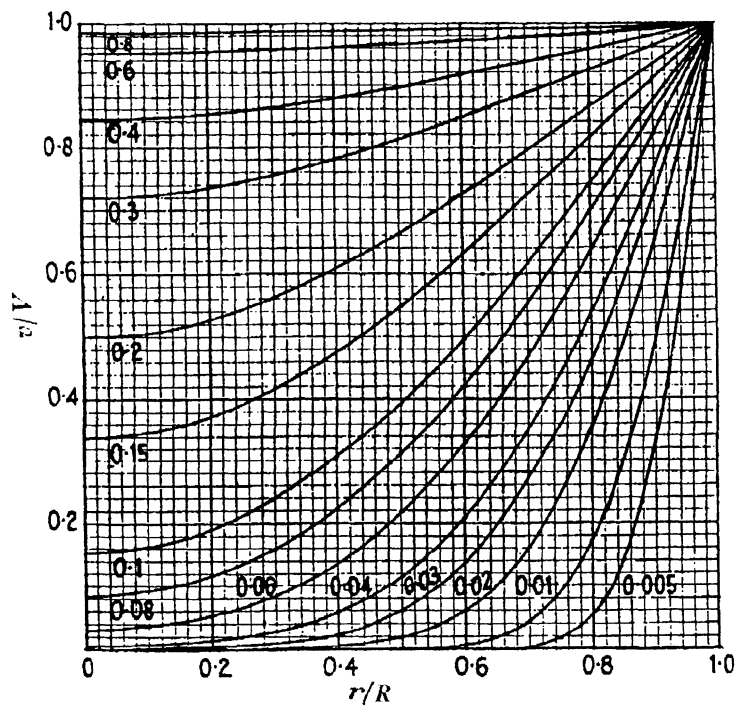


Fig. 8.6b. Radial heat conduction calculated analytically (from Ref. 27)

8.3.3 Line Source

The source term influence was examined by comparing the analytical and numerical solution for the line source problem.

The analytical solution to the heat equation with a continuous line source along the z-axis in an infinitely medium with an initial temperature of zero degrees yields [27].

$$T(r, t) = -\frac{q}{4\pi\lambda} E_i\left(-\frac{r^2}{4at}\right) \quad (8.26)$$

where q is the heat liberated per unit length per unit time.

E_i is the exponential integral equal to

$$-E_i(-x) = \int_x^{\infty} \frac{e^{-u}}{u} du \quad (8.27)$$

Numerical values of the exponential integral can be found in Jahnke-Emde, *Tables of functions* (Teubner, edn.3, 1933).

The analytical result for a medium with the same thermal conduction and thermal diffusivity constants as water ($a=0.6/4.18E6$, $\lambda=0.6$) is presented in Fig. 8.7.

The line source, q , produces 10 W/m.

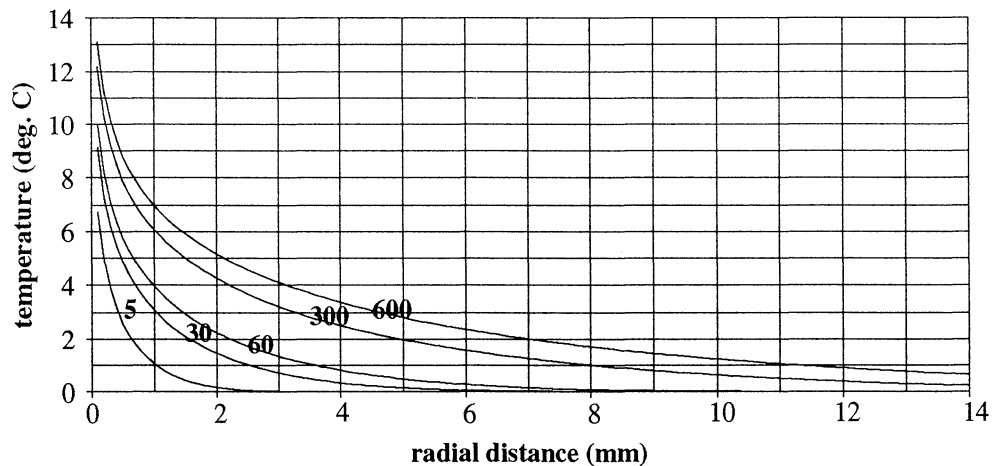


Fig. 8.7. Analytical solution to the heat conduction equation with a line source. The values on the curves are the time for which the solutions were calculated.

In the numerical model, an approximate line source was formed by introducing a cylinder with a radius of 0.1 mm on the symmetry axis. The solutions are presented in Fig. 8.8 with a heat production and heat transfer coefficients as for the previous solutions.

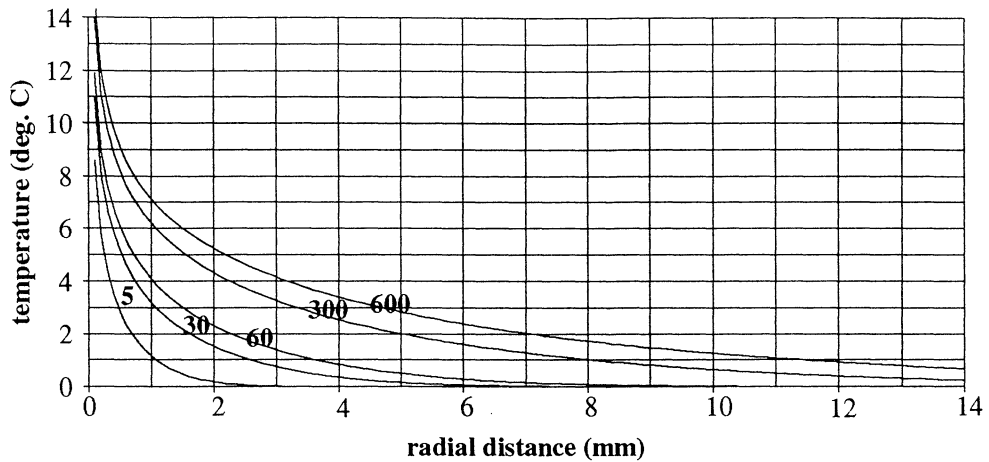


Fig. 8.8. Solutions to the line source problem calculated numerically.

8.3.4 Grid Size

In the model for laser-induced hyperthermia, the influence of the grid size to the results was investigated. The numerical solutions to the heat equation in a semi-infinite medium for different grid sizes were calculated. Using a medium with optical properties typical for tissue, Monte Carlo simulations with an infinitely narrow beam gave the source terms. The beam power was chosen to 5 W, the surface temperature was 25 °C, the initial temperature of the medium was 37 °C and the solutions were calculated after 180 s. Figs. 8.9-8.13 present the results obtained. Note that the solutions start a distance $\Delta z/2$ mm from the upper surface and a distance $\Delta r/2$ mm from the z-axis.

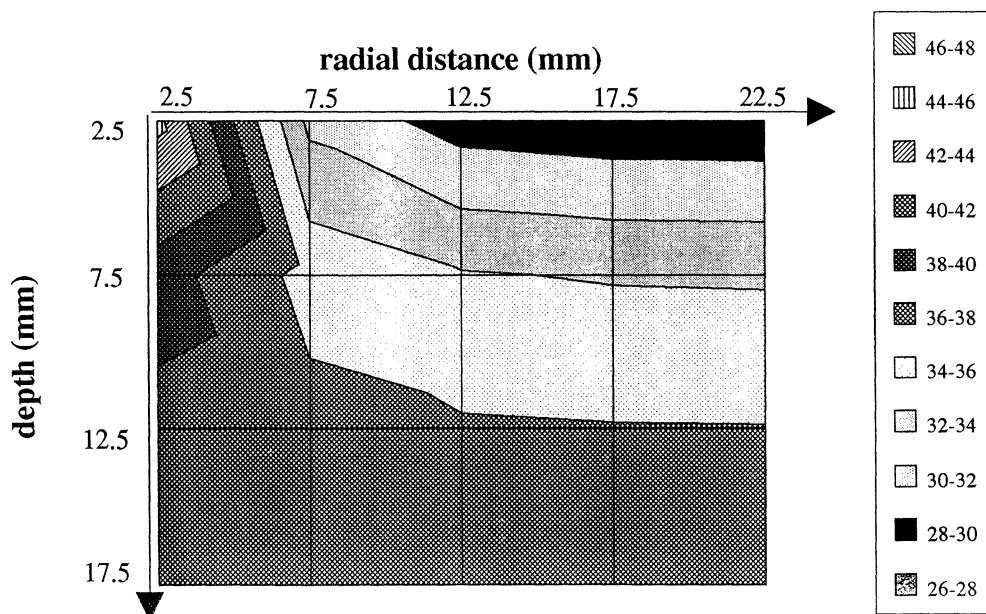


Fig. 8.9. The temperature distribution calculated for a grid size of $\Delta r = \Delta z = 5$ mm after 180 s for a medium with water-like heat transfer properties irradiated with a 5 W laser beam. The distance between two isotherms is two deg. C.

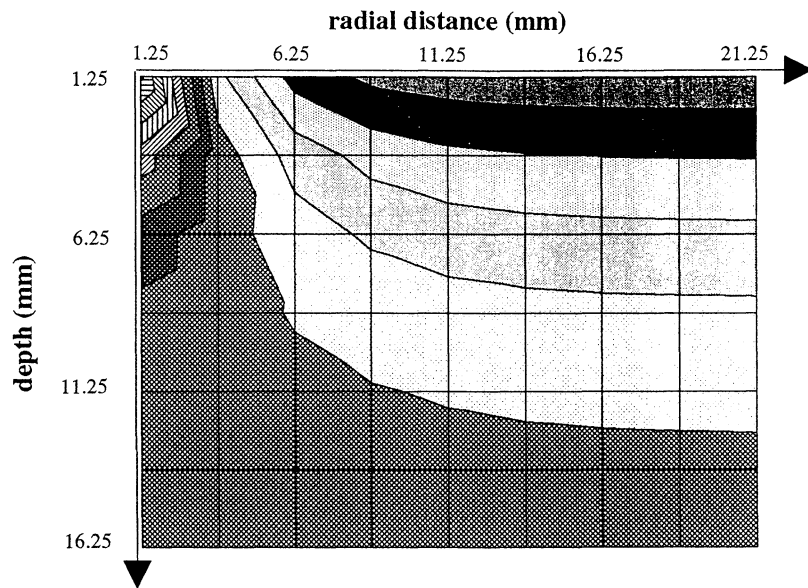


Fig. 8.10. The temperature distribution calculated for a grid size of $\Delta r = \Delta z = 2.5$ mm.

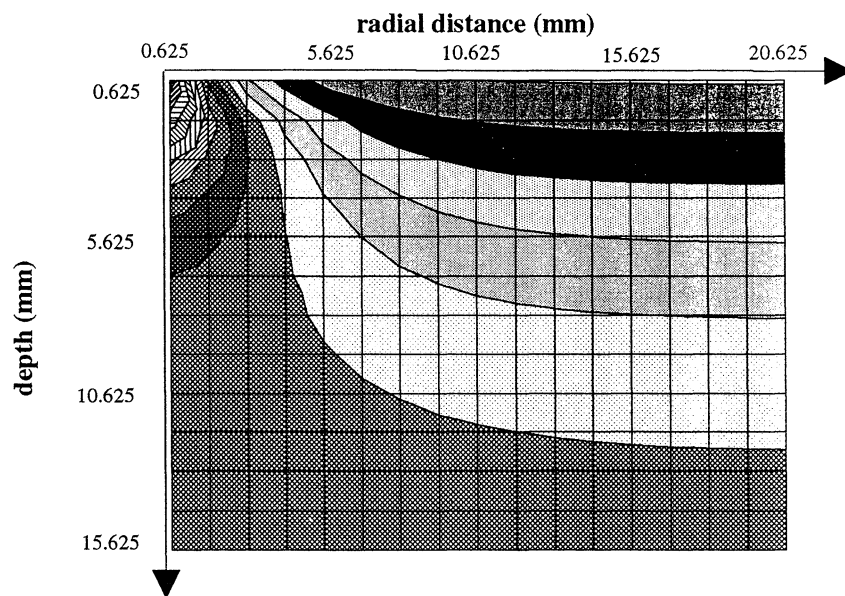


Fig. 8.11. The temperature distribution calculated for a grid size of $\Delta r = \Delta z = 1.25$ mm.

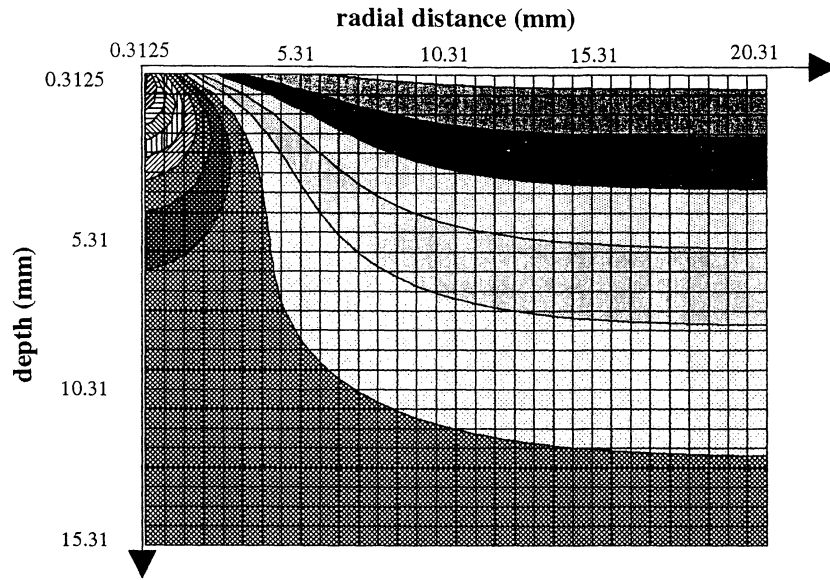


Fig. 8.12. The temperature distribution calculated for a grid size of $\Delta r = \Delta z = 0.625$ mm.

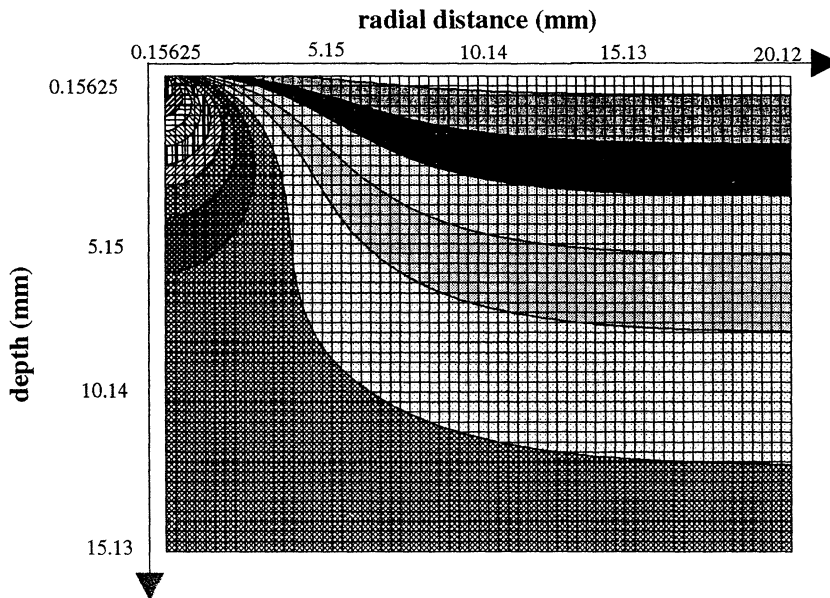


Fig. 8.12. The temperature distribution calculated for a grid size of $\Delta r = \Delta z = 0.3125$ mm.

It is clearly shown that the only effect resulting in decreasing the grid size will be a higher resolution of the temperature distribution.

9 Experimental Method

Experiments were performed where beef liver samples were irradiated by a laser and the temperature was measured at various points within the liver. The obtained temperature curves were then compared with the results obtained from the numerical model with conditions equivalent of the experimental situation.

9.2 Thermistor Calibration

The thermistors (Yellow Springs) utilised for the temperature measurements needed to be calibrated before usage. Temperature-changes alter the resistance of the thermistors. A certain resistance corresponds to a certain temperature.

For calibration of the thermistors, water in a tank was heated and was then let to cool off while being stirred. The thermistors were placed in close proximity to a digital thermometer placed into the tank. The resistances of the thermistors were measured when the thermometer showed a whole degree Celsius. A conversion table was then set up where the resistance was converted to a temperature. In Appendix B, the conversion program is presented. Following the instructions from the manufacturer of the thermistors, a linear interpolation was done between the calibration points.

9.1 Experimental Set-up

Two different lasers were used; an argon ion laser emitting light at 488 & 514 nm and a Nd:YAG laser emitting at 1064 nm.

The laser light was coupled through a 600 μm diameter fibre. The fibre tip was placed just above the liver surface, irradiating a spot of approximately the same area as the fibre tip. The output power was 1.4 W when using the Nd:YAG laser, and 500 mW for the argon ion laser.

Indirect temperature measurements were done using the micro thermistors described above. The thermistors was inserted through hollow needles which then were redrawn. The thermistors were inserted vertically from the approximately flat liver surface. The vertical distance from the fibre tip was then measured giving the r- coordinate of the measure point. After the treatment, the thermistor was stained at the liver surface with ink. Redrawing the thermistor, leaving a black mark where it had been inserted, made it possible to measure the inserted depth, giving the z- coordinate of the measure point.

The laser was switched on for 600 s and the temperature was registered every 15 s. After 900 s, the temperature measurements stopped.

With the Nd:YAG laser, an additional experiment was performed where a larger surface was irradiated. A microscope objective placed after the fibre tip expanded the laser beam. Temperature measurements were performed at two points; at the surface and at a depth of approximately 3 mm. The temperature probe (i.e. the thermistor) inside the liver was inserted in an almost horizontal fashion to avoid any temperature gradients over the measuring region of the temperature probe. Six measurement series were performed irradiating the liver surface with a top hat distribution with a diameter of 2.0 cm. The total power over the spot was 1.8 W. Temperature measurements proceeded for 1200 s, while the laser was switched off after 900 s.

10 Model Coefficients

The experimental temperature curves were compared to temperature curves provided by the heat transfer model. The absorption profile was furnished by the Monte Carlo simulations using values for native and coagulated liver tissue at 1064 nm [29] and native liver tissue at 488nm [30].

The optical parameters used were

		μ_a (mm ⁻¹)	μ_s (mm ⁻¹)	g
1064 nm.	native	0.05	8	0.97
	coag.	0.06	30	0.95
488 nm.	native	1.22	17.35	0.93

The heat transfer properties of the liver were estimated, as discussed below, to be:

$$\begin{aligned}\rho &= 1060 \text{ kg/m}^3 \\ c &= 3.67 \cdot 10^3 \text{ J/kg K} \\ \lambda &= 0.59 \text{ W/m K}\end{aligned}$$

The density and heat capacity values are based on the following experimentally derived relations for tissues [30]:

$$\begin{aligned}\rho &= (1.3 - 0.3W) \cdot 10^3 \text{ kg/m}^3 \\ c &= (0.37 + 0.67W/\rho) \cdot 4.19 \cdot 10^3 \text{ J/kg K}\end{aligned}$$

where W ($0 < W < 1$) is the water content, assumed for the liver to be 80 %.

The value of the heat conductivity was chosen equal to the heat conductivity of water at 15 °C.

The last value to be determined was the heat transfer resistance at the boundary liver / air. An experiment was performed where a liver sample was taken out of the refrigerator, having a uniform temperature, and was let to warm up with two temperature probes inserted at a depth of 3 mm. The numerical simulations were made to fit the obtained temperature curves (Fig 10.1). The surface resistance was in this way determined to 1/17 m²K/W.

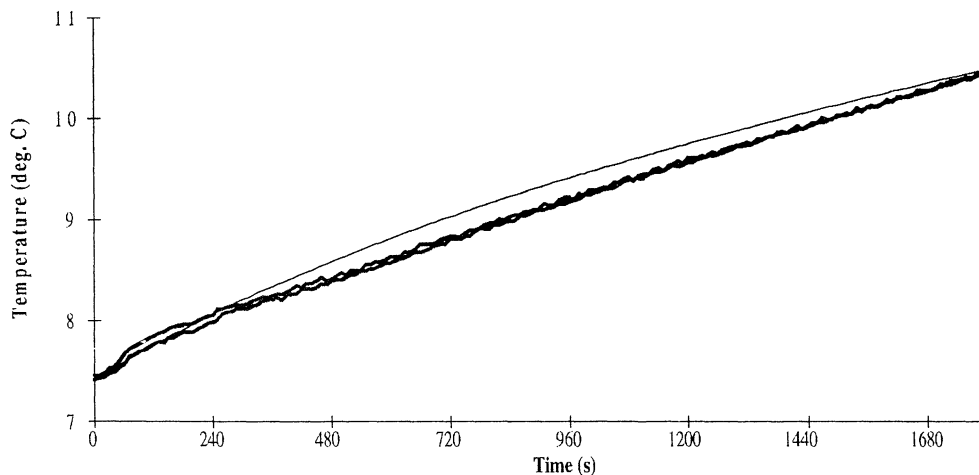


Fig. 10.1. Experimental (bold) curves and calculated curve calculated with $R_{\text{surface}} = 1/17 \text{ m}^2\text{K/W}$

11 Results

Simulations were performed with the above described optical and heat transfer coefficients. The simulation results was plotted with the experimentally obtained values to examine the validity of the model.

11.1 Nd:YAG Laser Results

With the laser fibre just above the liver sample, the temperature was recorded for three different points with a laser power of 1.4 W. Four measurements at each point were performed. Figs. 11.1-11.3 shows the experimental average temperature curves (bold line) with the standard deviation and the calculated temperature curves with a light absorption distribution for native and coagulated tissue. The light absorbed was calculated to be 1.15 W and 1.05 W for native and coagulated liver tissue respectively. This leads to a higher temperature for non-coagulated tissue at the observed points. Figs. 11.4a and b, show the fluence rate for native and coagulated tissue, respectively, simulated by the Monte Carlo program.

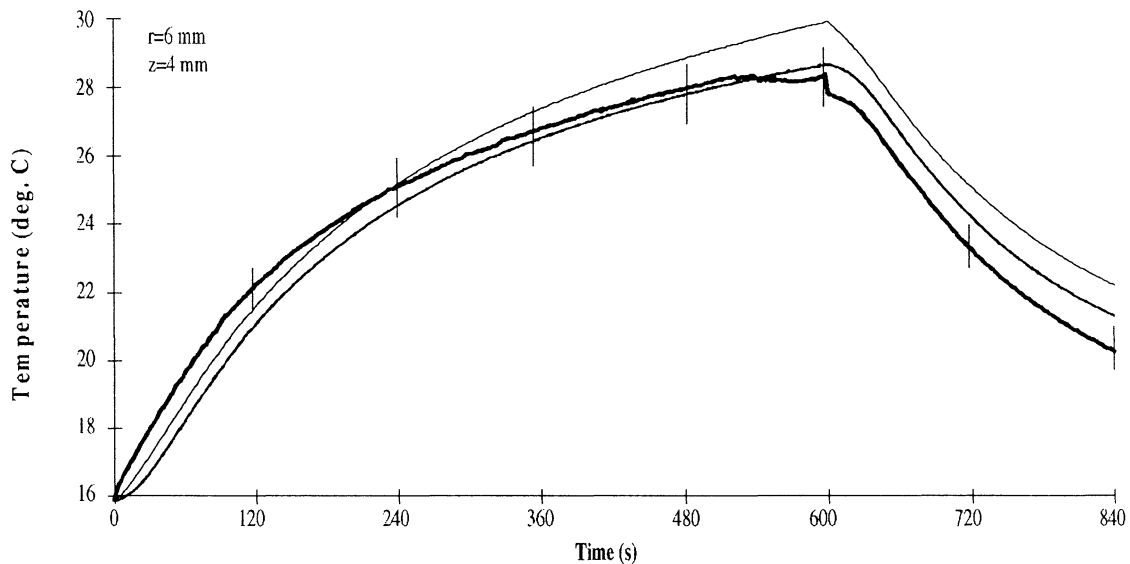


Fig. 11.1. Experimental (bold) and calculated curves at $r=6$ mm, $z=4$ mm.

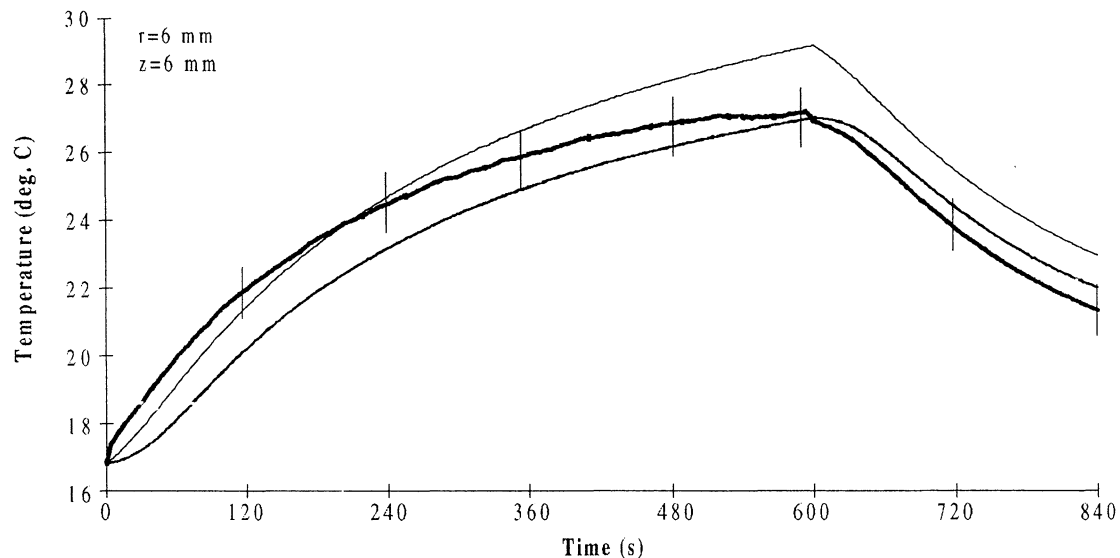


Fig. 11.2 Experimental (bold) and calculated curves at $r=6$ mm, $z=6$ mm.

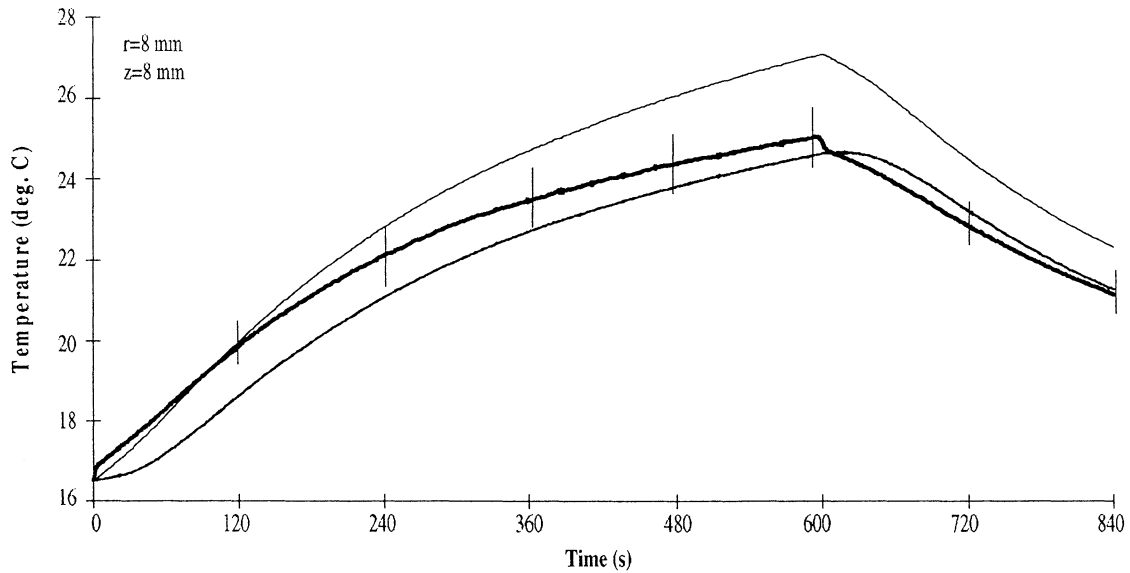


Fig. 11.3 Experimental (bold) and calculated curves at $r=8$ mm, $z=8$ mm.

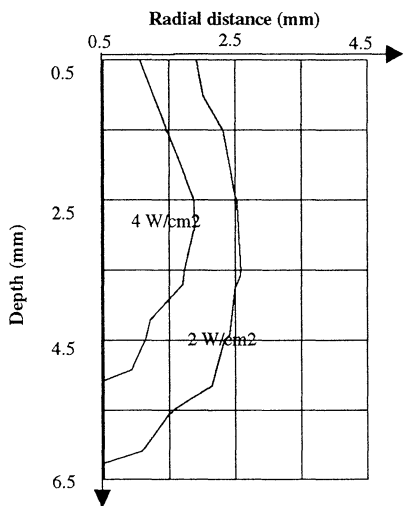


Fig. 11.4a. Calculated fluence rate for native tissue. Total beam power: 1.4 W.

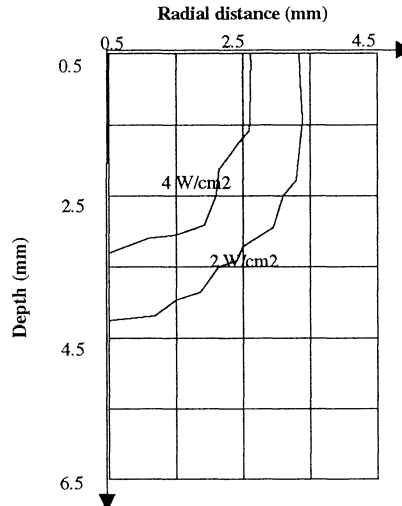


Fig. 11.4b. Calculated fluence rate for coagulated tissue. Total beam power: 1.4 W

Coagulation was observed to occur during the treatment. This will alter the absorption profile within the liver, and subsequently change the temperature distribution.

Based on visual observation of the coagulation, i.e. tissue whitening, the onset of coagulation was estimated to occur after 3 min of irradiation.

In Figs. 11.5-11.7, the same experimental curves as in the above figures are plotted with the simulated curves with coagulation occurring after 180 s.

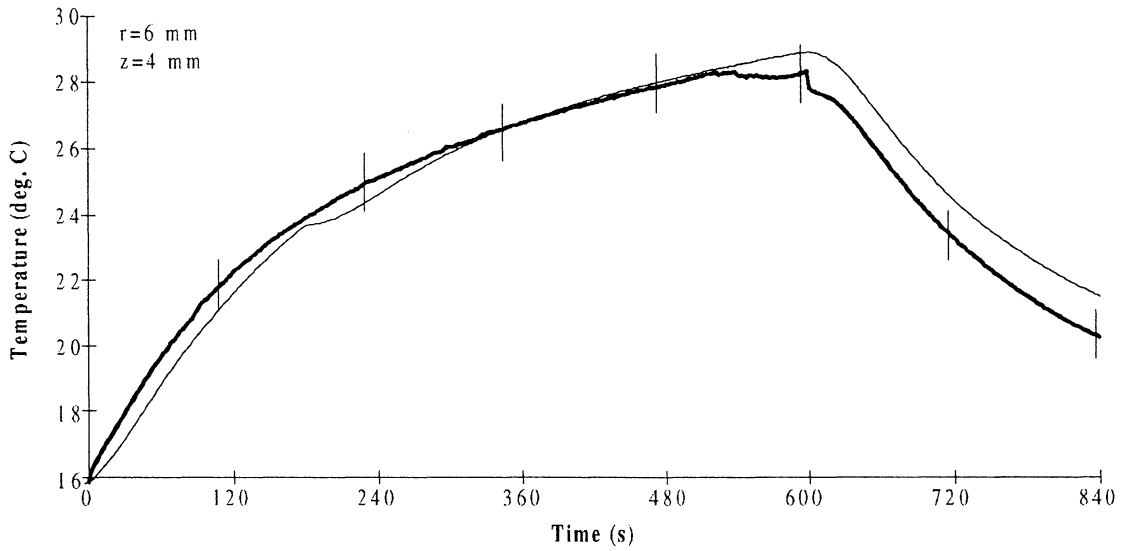


Fig. 11.5. Experimental (bold) and calculated curves with coagulation occurring after 180 s at $r=6 \text{ mm}$, $z=4 \text{ mm}$.

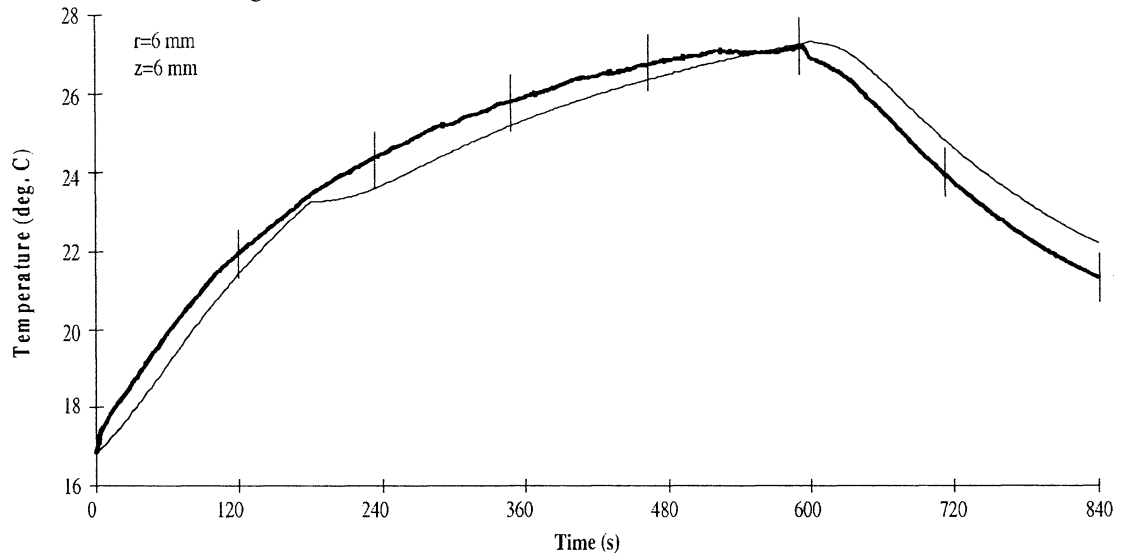


Fig. 11.6. Experimental (bold) and calculated curves with coagulation occurring after 180 s at $r=6 \text{ mm}$, $z=6 \text{ mm}$.

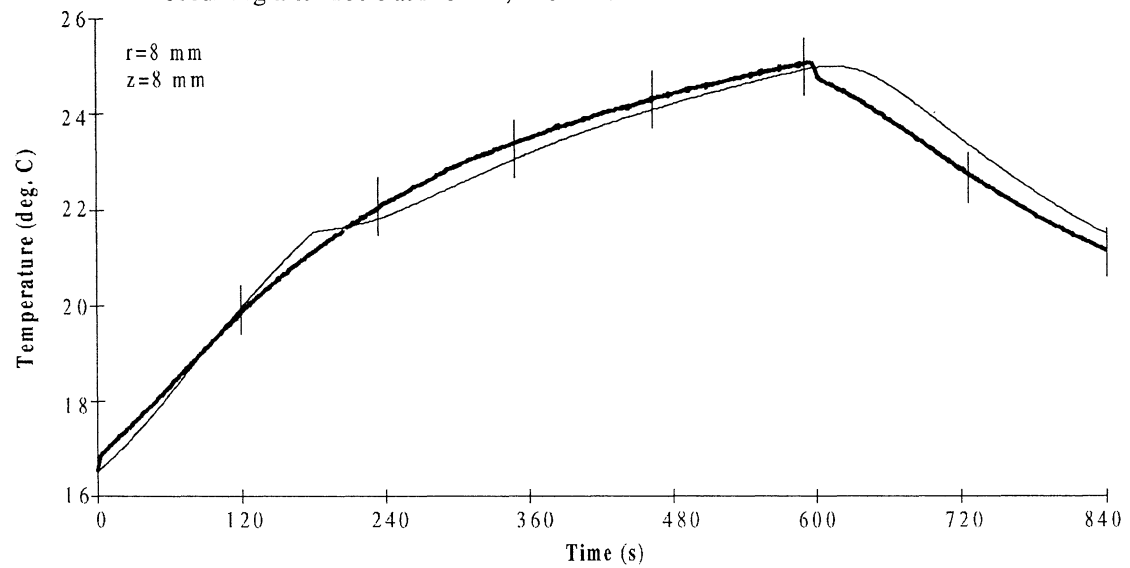


Fig. 11.7. Experimental (bold) and calculated curves with coagulation occurring after 180 s at $r=8 \text{ mm}$, $z=8 \text{ mm}$.

At one occasion, charring occurred at the fibre tip. Fig. 11.8. presents the recorded temperature curves with charring starting after 450 s.

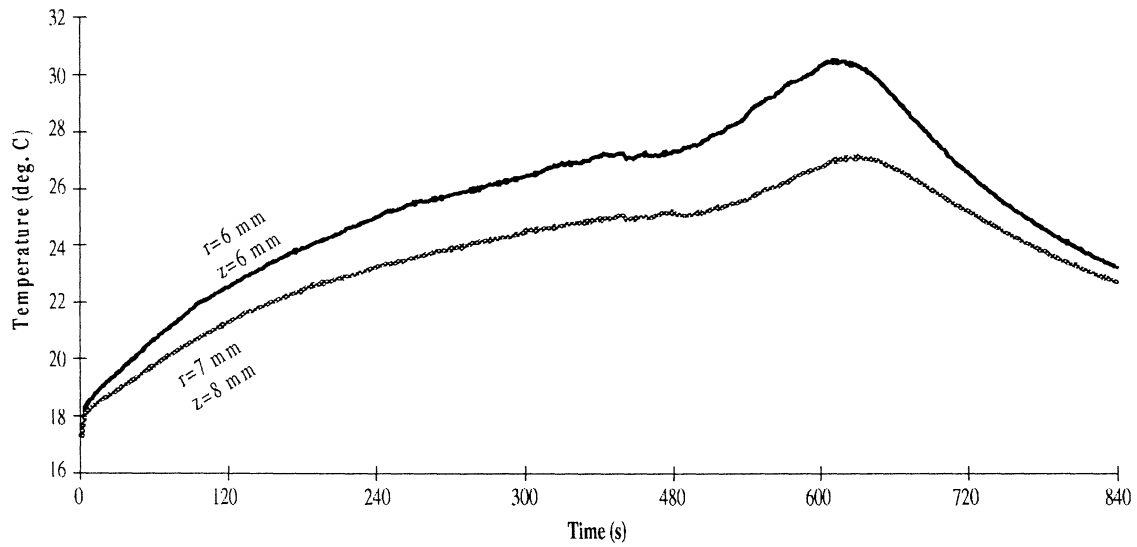


Fig. 11.8. Temperature recordings at $r=6\text{ mm}$, $z=6\text{ mm}$ and at $r=7\text{ mm}$, $z=8\text{ mm}$ with charring after 450 s.

As a second experiment, an area of 3.14 cm^2 on the liver was irradiated by a total beam power of 1.8 W. Temperature measurements were performed at the surface and at 3 mm of depth. Six experimental series were performed. Fig. 11.8 shows the fluence rate calculated by Monte Carlo simulations. The optical parameters used are those of native liver.

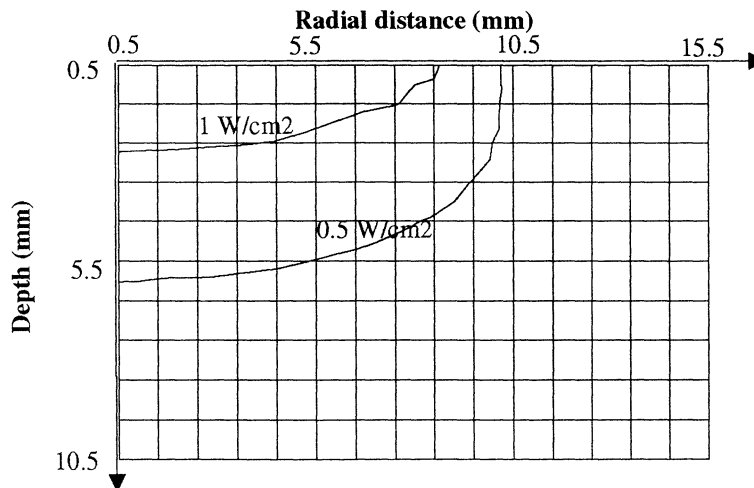


Fig. 11.8. Calculated fluence rate in the liver with a beam size diameter of 20 mm and a total beam power of 1.8 W.

Fig. 11.9 presents the experimental and calculated values for the above described situation.

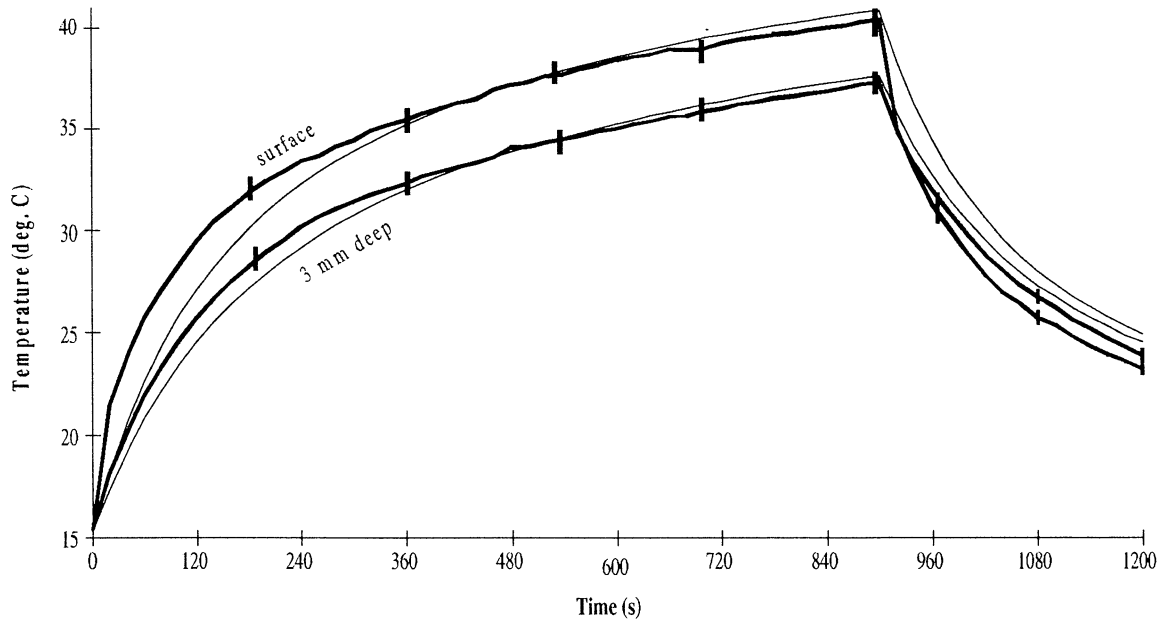


Fig. 11.9. Temperature at the surface and at 3 mm of depth. Experimental (bold) and calculated curves.

To examine the light absorption by the probes themselves, additional tests were performed where a thermistor was put into a glass of water, having a temperature of 17 °C. Irradiating the probe with 1064 nm light at 1.4 W, directly increased the probe temperature to 21-22 °C.

11.2 Argon Ion Laser Results

Experiments analogous to the first category Nd:YAG experiments were performed with an argon ion laser. The temperature at two different points were measured and compared to the corresponding calculated curves. A power of 500 mW was used.

Figs. 11.10-11.11 show the experimental and calculated curves for the two points.

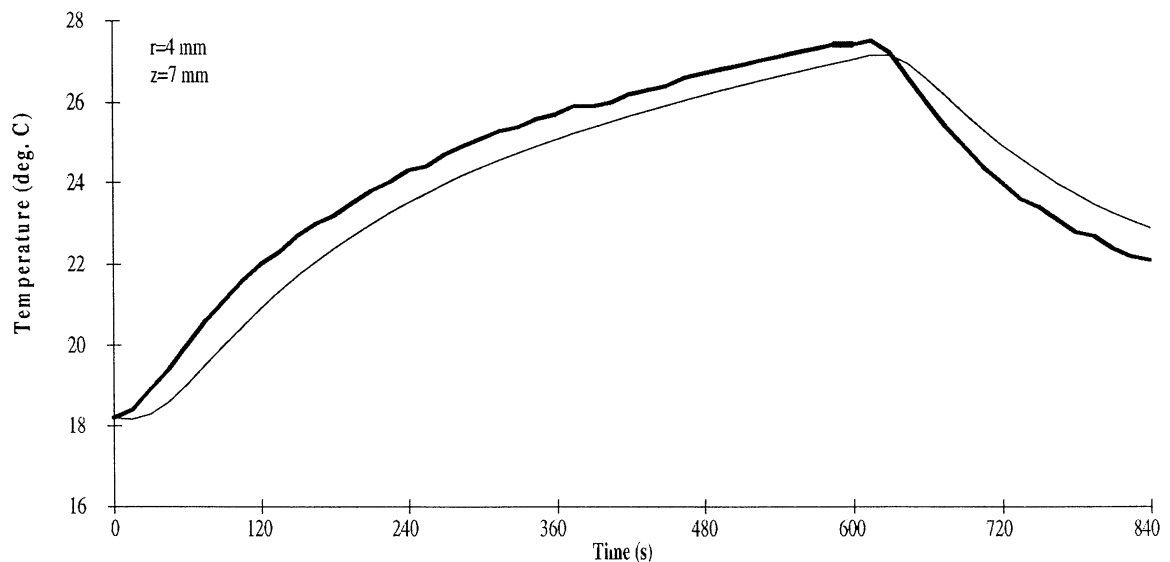


Fig. 11.10. Experimental (bold) and calculated curves at r=4 mm, z=7 mm.

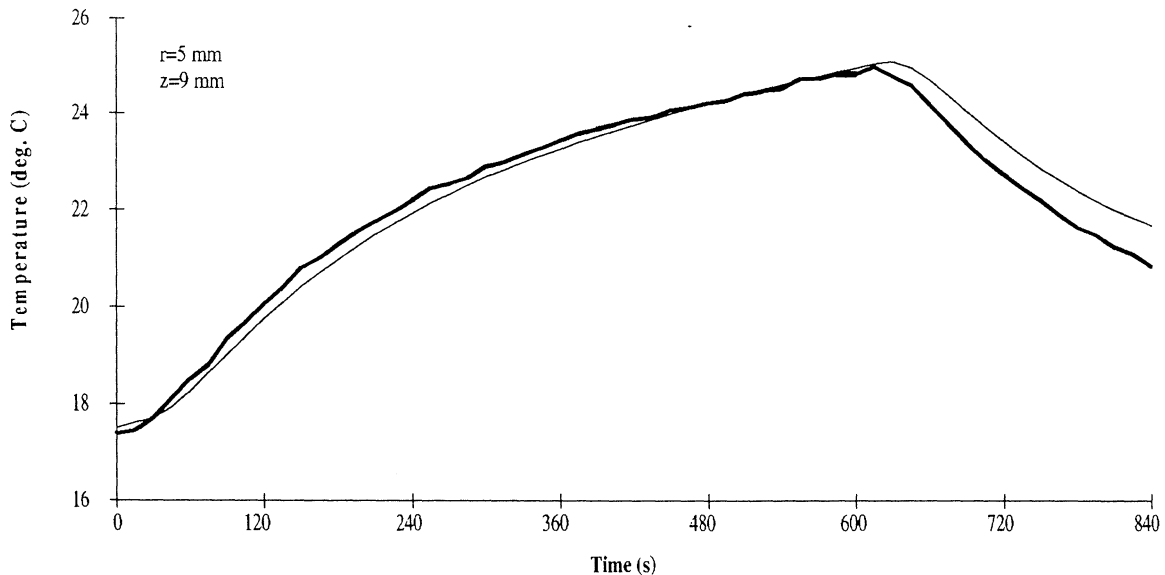


Fig. 11.11. Experimental (bold) and calculated curves at $r=5$ mm, $z=9$ mm.

12 Discussion and Conclusions

The results show that it is possible to predict the temperature in laser beam irradiated liver tissue with good accuracy.

12.1 Result Interpretation

Coagulation of tissue will change the optical properties significantly and thereby alter the temperature distribution. A first attempt to adjust for this in the calculations has been done. The introduction of coagulative optical coefficients after a certain visually derived time, proved to give a good agreement between model and experiment. Smoother simulated curves would be possible to obtain with a more sophisticated method of introducing the changing optical properties. In the present work, only two different set of optical parameters have been used. A natural step would now be to examine the alterations of these parameters as a function of time and temperature. Such results could then be used to generate a Monte Carlo simulation look-up table. The heat transfer program could then adjust the absorption profile within the tissue using this table.

In the model, the heat conductivity, heat capacity and tissue density are assumed to be constant, independent of the temperature. This is obviously not the case. To get an idea of the significance of this negligence, the example of water can be illustrative. Between 15 and 60 °C, the conductivity augment 10 %, whereas the density drops 2 % and the capacity rests almost unchanged. This results in a rise of the heat diffusivity by 12 %. It is plausible that the alteration of the thermal properties of liver tissue is of equal magnitude. In part, this can explain the divergence between the calculated and the experimental values after the laser has been switched off, as the cooling rate has been found to be higher in the experiments than in the model calculations.

In the expanded beam experiment (Fig. 11.9), the intensity distribution over the irradiated spot was assumed being flat, an assumption used when calculating the light absorption profile in the tissue.

The observed steep rise of the experimental surface temperature can be explained by light absorption by the temperature probe itself. This absorption was verified by an additional

test where the probe was irradiated with infrared light while in water. The recorded temperature augmentation could be assigned to following light absorption of the thermistor, as water scarcely absorbs at the laser wavelength.

The discrepancy between the predicted and the experimental values disappears when the probe reaches thermal equilibrium with the liver surface. As the light flux is smaller on the probe inserted at 3 mm of depth, the correspondence between calculated and experimental values is very good.

In the experiments using an argon ion laser, charring occurred almost instantaneously at the fibre tip due to the short penetration depth of green light. Charring will increase and spatially concentrate the absorption in the tissue. The absorption of the native liver was calculated to be 94 % with a very small spatial distribution. Therefore, the changing of the optical parameters was assumed to have only a marginal effect on the temperature distribution at the observed points. Thus, the temperature was calculated from native liver optical parameters.

12.2 Measurement Uncertainties

A general problem during the experiments has been the determination of the coordinates of the measure points. It should be possible to construct a mechanical support, where the measure point could be more correctly pre-determined. This uncertainty partly limited the smallest distance from the fibre tip at which measurements could be performed.

There is also a problem of heat conduction along the temperature probe itself. If the probe is inserted through a region warmer than the measurement point, the registered temperature can, by cause of conduction along the probe, be higher than the actual temperature.

In order to avoid any larger temperature gradients, the measurement points were chosen far away from the fibre tip. Inevitably, this poses the question of whether the temperature distributions closer to the irradiation spot can be correctly predicted by the model. It is not, though, advisable to envisage being able to measure very much closer to the irradiated spot with an acceptable degree of accuracy, as the temperature probes themselves do not have an infinitely small measuring region.

An indirect way of verifying the model in closer proximity of the fibre tip could be to examine the domain of the coagulative changes. These changes are more dependent of the instantaneous temperature than of the entire temperature history. Alternatively, a thermo camera could be used to measure the surface temperature close to the irradiated surface.

An alternative non-invasive temperature measurement technique is provided by nuclear magnetic resonance (NMR) [31].

12.3 The Influence of Charring

One experiment with the Nd:YAG laser induced charring of the tissue. Charring will increase the tissue absorption. Once charring has developed, a concentrated absorption will occur at that spot, heating it to induce charring of the surrounding areas. In this way an avalanche is launched. The higher absorption can readily be seen as a quick temperature rise in Fig. 11.8. Upon examination of the irradiated spot, as to be expected, the charred and the surrounding coagulated region was found to be much larger than when no charring occurred. This phenomenon of bigger, directly observable, tissue damages on charring has also been reported in interstitial experiments [32]. In this case the difference cannot be attributed to a higher degree of energy absorption, as no energy can escape the tissue. The observation can be explained as follows. When no charring

occurs, a large region will be heated up by light absorption. Thermal conduction will further allow the heat to dissipate to a large volume leading to a limited region of coagulated necrosis. In contrast, the more concentrated energy deposition occurring on charring induces larger coagulated areas. This can be ascribed to a drastically increased heat conduction ability and an extremely decreased heat capacity of charred tissue compared to untreated tissue. The outer regions of the charred area are thus quickly heated, leading to additional charring and a substantial circumferential coagulation. The dominant view up to now has been that charring should be avoided in laser photocoagulation to get greater tissue damages. With a more developed heat transfer model, adjusted to treat interstitial irradiation and a developed knowledge of the optical properties of charred tissue, it should be possible to elucidate this question more profoundly.

12.4 Future Prospects

The heat transfer model has proven to give solutions well in agreement with experimental results *in vitro*. What remains to be examined is the validity of the model compared to *in vivo* treatments. Blood flow will evidently influence the heat distribution. This factor is estimated to be the greatest of the components not considered in the model. Depending on the time of irradiation, refinements by various degrees of the model due to blood flow, may prove to be needed to get an acceptable accordance between model and experiment. A study examining the heat distribution *in vivo*, has been initiated.

To further develop the model, a more elaborate knowledge of how the optical properties change is desired. Studies on the influence of temperature and time of heating on the optical properties are scheduled in the near future. These results can then be incorporated into the model to get solutions corresponding even better with experiments. The knowledge of how heat influences cells, time of heating and temperature needed to get a desired response is continuously increasing within the project.

The major future goal, with this project as an initial study, is to provide a clinically useful therapeutic method of cancer based on hyperthermia. Even if much work remains to be done, it is my conviction that this goal can be attained in a not too distant future.

13 List of References

1. T.J. Dougherty, J.E. Kaufman, K.R. Weishaupt, D.G. Boyle and A. Mittelman, "Photoradiation therapy and treatment of malignant tumours," *Cancer Res.* **38**, 2628-2635 (1978)
2. A. Dahlman, A.G. Wile, R.G. Burns, R.G. Mason, F.M. Johnson and M.W. Berns, "Laser photoradiation therapy of cancer," *Cancer Res.* **43**, 430-434 (1983)
3. C.A. Perez and B. Emami, "Clinical trials with local (external and internal) irradiation and hyperthermia: current and future perspectives," *Radiol. Clin. North Am.* **27**, 525-542 (1989)
4. O. Dahl, "Interaction of hyperthermia and chemotherapy," Application of hyperthermia in the treatment of cancer, *Recent Results in Cancer Therapy* vol. 107, Springer-Verlag (1988)
5. S. Andersson-Engels, J. Johansson, D. Killander, E. Kjellén, M. Olivio, L.O. Svaasand, K. Svanberg and S. Svanberg, "Photodynamic therapy alone and in conjunction with near-infrared light-induced hyperthermia in human malignant tumours: a methodological case study," *Proc. SPIE* **908**, 116-125 (1988)
6. M.W. Berns, J. Coffey and A.G. Wile, "Laser photoradiation of cancer: possible role of hyperthermia", *Lasers Surg. Med.* **4**, 87-92 (1984)
7. T.S. Mang, "Combination studies of hyperthermia induced by the neodymium: yttrium-aluminium-garnet (Nd:YAG) laser as an adjuvant to photodynamic therapy," *Lasers Surg. Med.* **10**, 173-178 (1990)
8. B. Alberts, D. Bray, J. Lewis, M. Raff, K. Roberts and J.D. Watson "Molecular biology of the cell", second edition, Garland Publishing New York (1989)
9. G. Gitnick, D.R. LaBreque and F.G. Moody (eds.), "Diseases of the liver and the biliary tract," Mosely Year Book (1992)
10. Z. Amin, J.J. Donald, A. Masters, R. Kant, A.C. Steger, S.G. Brown and W.R. Lees, "Hepatic metastases: interstitial laser photocoagulation with real-time US monitoring and dynamic CT evaluation of treatment," *Radiology* **187**, 339-347 (1993)
11. P.D. Schneider, "Liver resection and laser hyperthermia," *Surg. Clin. North Am.* **72**, 623-639 (1992)
12. A.C. Steger, W.R. Lees, P. Shorvon, K. Walmsley and S.G. Brown, "Multiple-fibre low-power interstitial laser hyperthermia: studies in the normal liver," *Br. J. Surg.* **79**, 139-145 (1992)
13. L.O. Svaasand, "Photodynamic and photohyperthermic response of malignant tumours," *Med. Phys.* **12**, 455-461 (1985)
14. C. Streffer, "Aspects of metabolic change after hyperthermia," Application of hyperthermia in the treatment of cancer, *Recent Results in Cancer Therapy* vol. 107, Springer-Verlag (1988)
15. J.A. Parrish and T.F. Deutsch, "Laser photomedicine," *IEEE J. Quant. Electron.* **QE-20**, 1386-1396 (1984)
16. S. Thomsen, "Pathologic analysis of photothermal and photomechanical effects of laser-tissue interactions, a review article," *Photochem. Photobiol.* **53**, 825-835 (1991)
17. H. Jung and E. Dikomey, "Some basic effects in cellular thermobiology," Application of hyperthermia in the treatment of cancer, *Recent Results in Cancer Therapy* vol. 107, Springer-Verlag (1988)

18. P. Vaupel, F. Kalinowski and M. Kluge, "Pathophysiology of tumors in hyperthermia," Application of hyperthermia in the treatment of cancer, Recent Results in Cancer Therapy vol. 107, Springer-Verlag (1988)
19. K. Dowlatshahi, D. Babich, J.D. Bangert and R. Kluiber, "Histologic evaluation of rat mammary tumor necrosis by interstitial Nd:YAG laser hyperthermia," Lasers Surg. Med. **12**, 159-164 (1992)
20. P.F. Turner and T. Schaefermeyer, "Technical aspects of hyperthermia," Application of hyperthermia in the treatment of cancer, Recent Results in Cancer Therapy vol. 107, Springer-Verlag (1988)
21. S.L. Jacques, "Laser-tissue interactions," Surg. Clin. North Am. **72**, 531-558 (1992)
22. A. Ischimarū, "Wave propagation and scattering in random media," Academic Press, New York (1978)
23. P. Kubelka, "New contributions to the optics of intensely light-scattering materials. Part I," J. Opt. Soc. Am. **38**, 448-457 (1948)
24. E. Hecht, "Optics," second edition, Addison-Wesley, (1987)
25. S.T. Flock, M.S. Patterson, B.C. Wilson and D.R. Wyman, "Monte Carlo modeling of light propagation in highly scattering tissues-I: model predictions and comparison with diffusion theory," IEEE Transact. Biomed. Eng. **36**, 1162-1168 (1989)
26. L.O. Svaasand, T. Boerlind and M. Oeveraasen, "Thermal and optical properties of living tissue: application to laser-induced hyperthermia," Lasers Surg. Med. **5**, 589-602 (1985)
27. H.S Carslaw and J.C. Jaeger, "Conduction of heat in solids," second edition, Oxford University Press (1959)
28. J. Dowden, M. Davis, P. Kapadia and K. Matthewson, "Heat flow in laser treatment by local hyperthermia," Lasers Med. Sci. **2**, 211-221 (1987)
29. A. Roggan, O. Minet, C. Schröder and G. Müller, "Measurements of optical properties of tissue using integrating sphere technique," Medical Optical Tomography: Functional Imaging and Monitoring, SPIE Optical Engineering Press (1993)
30. P. Parsa, S.L. Jaques and N.S. Nishioka, "Optical properties of rat liver between 350 and 2200 nm," Appl. Opt. **28**, 2325-2330 (1989)
31. A.S. Hall, M.V. Prior, J.W. Hand, I.R. Young and R.J. Dickinson, "Observation by MR imaging of in vivo temperature changes induced by radio frequency hyperthermia," J. Comp. Assist. Tomogr. **14**, 430-436 (1990)
32. Z. Amin, G. Buonaccorci, T. Mills, S. Harries, W.R. Lees and S.G. Bown, "Interstitial laser photocoagulation: evaluation of a 1320 nm Nd-YAG and an 805 nm diode laser: the significance of charring and the value of pre-charring the fiber tip," Laser Med. Sci. **8**, 113-120 (1993)

Appendix A

Heat Transfer Source Code (Borland C)

```
/*
-----
Temperature-distribution calculation
in radial and z direction
-----
*/
#include <alloc.h>
#include <process.h>
#include <string.h>
#include <stdio.h>
#include <math.h>
#include <stdlib.h>
/*****
/* The following values must be specified before takeoff */
#define laserwatt 1.4
#define thermcond 0.59
#define hcap 3.886E6
#define bordertemp 21.5
#define resist 0.0588235
#define ownstep 1
/*****
/*****
#define PI 3.1415926535
#define sqr(a) ((a)*(a))
void initial_conditions(void);
float *AllocVector(short nl, short nh);
float **AllocMatrix(short ncl,short nch,
                    short nrl,short nrh);
void FreeVector(float *v,short nl);
void FreeMatrix(float **m,short ncl,short nch,
                short nrl);
void nerror(char error_text[]);
void communicate(void);
void initdrdzq(void);
void init_allocation(void);
void heat_conductances(void);

void inverted_heatcapacities(void);
void stability_timestep(void);
void heat_flows(void);
void new_temperatures(void);
void resultout(void);
void no_source(void);
void release_memory(void);
void initwriteinterval(void);
void intervalwrite(void);
void extra(void);
float dz,dr;
short Jmax,Imax,Timeinterval,flag,tchoise;
short ljust,ljusti,off,countz[25],count[25],nrpoints;
float timet,timestep,maxtime,timestab,tinterval;
float irr_time,inittemp;
float **source;
float **temp;
float **hcapinv;
float **kondr;
float **kondz;
float **flowr;
float **flowz;
float *vol;
div_t truck;
char name_of_file[25];
char result_file[25];
void main(void)
{
    initdrdzq();
    communicate();
    init_allocation();
    initial_conditions();
    heat_conductances();
    inverted_heatcapacities();
    stability_timestep();
    if(tchoise==2)
    {
        flag=0;
        initwriteinterval();
        do {
            flag++;
            no_source();

```

```

        heat_flows();
        new_temperatures();
        truck=div(flag,Timeinterval);
        if(truck.rem==0)
            intervalwrite();
        if(flag==180)
            extra();
        timet += timestep;
    } while (timet <= maxtime);
}
else
{
do
    {
        no_source();
        heat_flows();
        new_temperatures();
        timet += timestep;
    } while (timet <= maxtime);
resultout();
}
release_memory();
}

void initdrdq(void)
{
    FILE *searcher;
    char strng2 [80],strtemp[30],strtempz[30];
    int i,j,length;
    double phot_dens,specula_reflec;
    float tempr,tempz;
    printf("_____
    _____\n\n");
    printf("      Temperature Calculation\n");
    printf("_____
    _____\n\n");
    printf("Searchpath plus name of file from M-C program.\n");
    printf("ex c:\mclib\frommc.mco\n");
    scanf("%s",name_of_file);
    searcher=fopen(name_of_file,"r");
    if (searcher != NULL)
{
do
    {
        fgets(strng2,81,searcher); /* The coming lines is
        specific to the file given by Monte-Carlo program */
        length=strlen(strng2);
    }
    while(!((strng2[(length-4)]== 111) && (strng2[(length-
    3)] == 110) && (strng2[(length-2)] == 115)));
    fscanf(searcher,"%f",&dz);
    fscanf(searcher,"%f",&dr);
    dr=dr/100; /* This program uses SI units */
    dz=dz/100;
    fgets(strng2,81,searcher);
    fscanf(searcher,"%d",&ljusj);
    fscanf(searcher,"%d",&ljusti);
    printf("\nDimensions of cells: dr=%3.2f dz=%3.2f
    [mm]\n",dr*1000,dz*1000);
    printf("Write area of interest in [mm]\n");
    printf("r direction:");
    scanf("%f",&tempr);
    printf("z direction:");
    scanf("%f",&tempz);
    tempr=tempr/dr/1000; /* We use a whole number of
    boxes.*/
    tempz=tempz/dz/1000; /* Relgating if input area isn't */
    gcvt(tempr,5,strtemp); /* just that. */
    gcvt(tempz,5,strtempz);
    Imax=atoi(strtemp);
    Jmax=atoi(strtempz);

    if ((Jmax<ljustj) || (Imax<ljusti))
    {
        printf("Defined dimensions must be greater
        than the ones \nused in the MC
        program");
        fclose(searcher);
        exit(1);
    }
}
do
    fgets(strng2,81,searcher);
while(!((strng2[0] == 82) && (strng2[1] == 65) &&
(strng2[2]==84))); /* A row beginning with 'RAT' if found */

```

```

fscanf(searcher,"%lf",&specula_reflec); /* Specular
reflectance */
do /* if correction wanted */
    fgets(strng2,81,searcher);
while(!((strng2[0] == 65) && (strng2[1] == 95)&&
(strng2[2]==114) &&
(strng2[3]==122))); /* A row beginning with 'A_rz' if
found */
source=AllocMatrix(1,Imax,1,Jmax); /* Allocate
memory for source terms */
for (i=1; i<=ljusi; i++)
    for (j=1; j<=ljusj; j++)
    {
        fscanf(searcher,"%lf",&phot_dens); /* Prob. of
absorp. per cubic cm */
        source[i][j]=phot_dens*1E6*laserwatt;
        /*Sourceterms */
    }
fclose(searcher);
}
else
{
    printf("File %s not found",name_of_file);
    exit(1);
}
}

void communicate()
{
    float rcord,zcord;
    float phot_dens;
    short i,j;
    FILE *searcher;
    printf("\nSearchpath plus name of resultfile.\n");
    scanf("%s",result_file);
    printf("\nTemperature calculation 1) area after a certain time");
    printf("\n                2) point at a certain time interval\n");
    printf("                ");
    scanf("%d",&tchoise);
    if(tchoise==2)
    {
        printf("\nNumber of points ");
        scanf("%d",&nrpoints);
        for(i=1;i<=nrpoints;i++)
        {
            printf("\nr-coordinate of point %d [mm] ",i);
            scanf("%f",&rcord);
            countr[i]=0;
            do
                countr[i]++;
            while((rcord/1000>countr[i]*dr) &&
(countr[i]*dr<Imax));
            printf("z-coordinate of point %d [mm] ",i);
            scanf("%f",&zcord);
            countz[i]=0;
            do
                countz[i]++;
            while((zcord/1000>countz[i]*dz) &&
(countz[i]*dz<Jmax));
        }
        printf("\nTime interval between registrations
[s] ");
        scanf("%f",&tinterval);
    }
    printf("Irradiation time [s]: ");
    scanf("%f",&irr_time);
    printf("\nInvestigation time [s]: ");
    scanf("%f",&maxtime);
    printf("\nInitial temperature [deg. C]: ");
    scanf("%f",&inittemp);
    searcher=fopen("a:ndyagre.arz","r");
    if(searcher==NULL)
        exit(1);
    for(i=1;i<36;i++)
        for(j=1;j<35;j++)
        {
            fscanf(searcher,"%f",&phot_dens); /* Prob.
of absorp. per cubic cm */
            source[i][j]=phot_dens*1E6*laserwatt;
        }
    fclose(searcher);
}

void init_allocation(void) /* Allocate big matrices */

```

```

    {
        vol=AllocVector(1,Jmax);
        kondr=AllocMatrix(1,Imax+1,1,Jmax+1);
        kondz=AllocMatrix(1,Imax+1,1,Jmax+1);
        flowr=AllocMatrix(1,Imax+1,1,Jmax+1);
        flowz=AllocMatrix(1,Imax+1,1,Jmax+1);
        hcapinv=AllocMatrix(1,Imax,1,Jmax);
        temp=AllocMatrix(1,Imax,1,Jmax);
    }

void initial_conditions(void)
{
    int i,j;
    for(i=1;i<(Imax+1);i++)
        for(j=1;j<(Jmax+1);j++)
            temp[i][j] = inittemp;

    timet = 0.0;
    for(i=2;i<(Imax+1);i++)
        vol[i]=PI*(sqr(i*dr)-sqr((i-1)*dr))*dz; /* Volume calc. for the cells */
    vol[1]=PI*dz*sqr(dr);
    off=0;
}

void heat_conductances(void)
{
    int i,j;
    for(j=1;j<(Jmax+1);j++)
    {
        kondr[1][j] = 0.0; /* Symmetry */
        kondr[(Imax+1)][j] = 0.0; /* Insulated */
    }
    for(i=2;i<(Imax+1);i++)
        for(j=1;j<(Jmax+1);j++)
            kondr[i][j] = 2.0*PI*dz/
                (log((i-1)*dr/((i-1)*dr-dr/2))/thermcond+
                 log(((i-1)*dr+dr/2)/((i-1)*dr))/thermcond);
    for(i=1;i<(Imax+1);i++)
    {
        kondz[i][1] = PI*(sqr(i*dr)-sqr((i-1)*dr))/
            ((dz/2)/thermcond+resist);
        kondz[i][(Jmax+1)] = 0.0; /* Insulated */
    }
    for(i=1;i<(Imax+1);i++)
        for(j=2;j<(Jmax+1);j++)
            kondz[i][j] = PI*(sqr(i*dr)-sqr((i-1)*dr))/
                ((dz/2)/thermcond +
                 (dz/2)/thermcond);
}

void inverted_heatcapacities(void)
{
    register short i,j;
    for(i=1;i<(Imax+1);i++)
        for(j=1;j<(Jmax+1);j++)
            hcapinv[i][j] = 1.0/(hcap*vol[i]);
}

void stability_timestep(void)
{
    float test, maxtest;
    register short i,j;
    char strtempt[30];
    maxtest = 0.0;
    for(i=1;i<(Imax+1);i++)
    {
        for(j=1;j<(Jmax+1);j++)
        {
            test = hcapinv[i][j]*
                (kondr[i][j]+kondr[i+1][j] +
                 kondz[i][j]+kondz[i][j+1]);
            if (test > maxtest) maxtest = test;
        }
    }
    timestep = 0.99/maxtest;
    if (ownstep<timestep)
        timestep=ownstep;
    printf("stability time-step = %2.4f sec.\n",timestep);
    if (tchose==2)
    {
        tinterval=tinterval/timestep;
        gcvt(tinterval,5,strtempt);
        Timeinterval=atoi(strtempt);
    }
}

```

```

void heat_flows(void)
{
    register short i,j;
    for(i=1;i<(Imax+1);i++)
        {
            flowz[i][1] = kondz[i][1]*(bordertemp-temp[i][1]);
            flowz[i][(Jmax+1)] = 0.0;
        }
    for(i=1;i<(Imax+1);i++)
        for(j=2;j<(Jmax+1);j++)
            flowz[i][j] = kondz[i][j] *(temp[i][j-1]-temp[i][j]);

    for(j=1;j<(Jmax+1);j++)
        {
            flowr[1][j] = 0.0;
            flowr[(Imax+1)][j] = 0.0;
        }
    for(i=2;i<(Imax+1);i++)
        for(j=1;j<(Jmax+1);j++)
            flowr[i][j] = kondr[i][j] *(temp[i-1][j]-temp[i][j]);
}

```

```

void new_temperatures(void)
{
    register short i,j;
    for(i=1;i<(Imax+1);i++)
        for(j=1;j<(Jmax+1);j++)
            temp[i][j] +=
                hcapinv[i][j]*(flowr[i][j]-flowr[i+1][j] +
                flowz[i][j]-flowz[i][j+1]+source[i][j]*vol[i])*timestep;
}

```

```

void resultout(void)
{
    FILE *givare;
    short i,j;
    float dist;
    dr=dr*1000;
    dz=dz*1000;
    givare=fopen(result_file,"w");
}

```

fprintf(givare,"Result file\nThe first row and column gives the middle\ncoordinates of that cell in [mm]\nThe matrix gives the temperature in deg C\n");

```

fprintf(givare,"\n%d",0);
for(i=1;i<(Imax+1);i++)
{
    dist=(i-1)*dr+dr/2;
    fprintf(givare,"%t%3.3f",dist);
}
fprintf(givare,"\n");
for(j=1;j<(Jmax+1);j++)
{
    dist=(j-1)*dz+dz/2;
    fprintf(givare,"%3.3f",dist);
    for(i=1;i<(Imax+1);i++)
        fprintf(givare,"%t%f",temp[i][j]);
    fprintf(givare,"\n");
}
fclose(givare);
}

```

```

void initwriteinterval(void)
{
    short i;
    FILE *givare;
    givare=fopen(result_file,"w");
    fprintf(givare,"Result file\nTemperature calculated at \n");
    fprintf(givare,"Time");
    for(i=1;i<=nrpoints;i++)
        fprintf(givare,"\tr=%3.2f z=%3.2f", (countz[i]*dr-dr/2)
            *1000, (countz[i]*dz-dz/2)*1000);

    fprintf(givare,"\n0t");
    for(i=1;i<=nrpoints;i++)
        fprintf(givare,"%3.2ft", inittemp);
    fprintf(givare,"\n");
    fclose(givare);
}

```

```

void intervalwrite(void)
{
    short i;
}

```

```

        FILE *givare;
        givare=fopen(result_file,"a");
        fprintf(givare,"%3.1f\t",timet+ timestep);
        for(i=1;i<=nrpoints;i++)
            fprintf(givare,"%3.3f\t",temp[coutnr[i]][countz[i]]);
        fprintf(givare,"\n");
        fclose(givare);
    }

void no_source(void)
{
    int ij;
    if((timet>=irr_time) && (off!=1))
    {
        for(j=1;j<(Jmax+1);j++)
            for(i=1;i<(Imax+1);i++)
                source[i][j]=0.0;

        off=1;
    }
}

void extra(void) /*Routine for changing the absorption coefficients*/
{
    FILE *searcher;
    short ij;
    double phot_dens;
    char strng2 {80};
    searcher=fopen("a:ndyagco.mco","r");
    do /* if correction wanted */
        fgets(strng2,81,searcher);
    while(!((strng2[0] == 65) && (strng2[1] == 95)&& (strng2[2]==114) &&
        (strng2[3]==122))); /* A row beginning with 'A_rz' if
        found */

    for (i=1; i<=ljusi; i++)
        for (j=1; j<=ljusj; j++)
        {
            fscanf(searcher,"%lf",&phot_dens); /* Prob. of absorp. per cubic
            cm */
            source[i][j]=phot_dens*1E6*laserwatt; /* Sourceterms */
        }
    fclose(searcher);
}

```

```

void release_memory(void)
{
    FreeVector(vol,1);
    FreeMatrix(kondr,1,Imax+1,1);
    FreeMatrix(kondz,1,Imax+1,1);
    FreeMatrix(flowr,1,Imax+1,1);
    FreeMatrix(flowz,1,Imax+1,1);
    FreeMatrix(temp,1,Imax,1);
    FreeMatrix(hcapinv,1,Imax,1);
    FreeMatrix(source,1,Imax,1);
}

/*****
 * Report error message to stderr, then exit the program
 * with signal 1.
 *****/
void nerror(char error_text[])
{
    fprintf(stderr,"%s\n",error_text);
    fprintf(stderr,"...now exiting to system...\n");
    exit(1);
}

/*****
 * Allocate an array with index from nl to nh inclusive.
 *
 * Original matrix and vector from Numerical Recipes in C
 * don't initialize the elements to zero. This will
 * be accomplished by the following functions.
 *****/
float *AllocVector(short nl, short nh)
{
    float *v;
    short i;

    v=(float *)malloc((unsigned) (nh-nl+1)*sizeof(float));
    if (!v) nerror("allocation failure in vector()");

    v -= nl;
    for(i=nl;i<=nh;i++) v[i] = 0.0; /* init. */
    return v;
}

```

```

}

/*****
* Allocate a matrix with row index from nrl to nrh
* inclusive, and column index from ncl to nch
* inclusive.
*****/
float **AllocMatrix(short ncl,short nch,
                    short nrl,short nrh)
{
    short i,j;
    float **m;

    m=(float **) malloc((unsigned) (nch-ncl+1)
                        *sizeof(float*));

    if (!m) perror("allocation failure 1 in matrix()");
    m -= ncl;

    for(i=ncl;i<=nch;i++) {
        m[i]=(float *) malloc((unsigned) (nrh-nrl+1)
                               *sizeof(float));

        if (!m[i]) perror("allocation failure 2 in matrix()");
        m[i] -= nrl;
    }

    for(i=ncl;i<=nch;i++)
        for(j=nrl;j<=nrh;j++) m[i][j] = 0.0;
    return m;
}

/*****
* Release the memory.
*****/
void FreeVector(float *v,short nl)
{
    free((char*) (v+nl));
}

```

```

/*****
* Release the memory.
*****/
void FreeMatrix(float **m,short ncl,short nch,short nrl)
{
    short i;

    for(i=nch;i>=ncl;i--) free((char*) (m[i]+nrl));
    free((char*) (m+ncl));
}

```

Appendix B

Temperature Conversion Source Code (Borland C)

```
#include <alloc.h>
#include <process.h>
#include <string.h>
#include <stdio.h>
#include <math.h>
#include <stdlib.h>
#include <conio.h>
void resultout(void);
void conversion(void);
void init(void);
float probe1,probe2;
int timestep,r1,z1,r2,z2,laseroff;
float temp1,temp2;
float
resist1[80]={3420,3260,3180,3050,2940,2830,2730,2640,2560,2470,2380,2300,2210,2130,2060,199
3,1928,1863,1796,1760,1718,1632,1578,1521,1482,1440,1397,1360,1321,1274,1186,1151,1117,108
3,1051,1021,988,963,934,907,880,856,832,809,787,767,747,725,705,688,670,652,634,619,603,587,5
73,558,543,529,519,503,489,479,467,455,445,430,421,418,405,394,383,377,365,358,351,342,332};
float
resist2[80]={3670,3500,3420,3280,3126,3007,2896,2804,2719,2608,2513,2423,2328,2247,2170,209
8,2029,1968,1897,1811,1767,1670,1619,1568,1519,1473,1428,1390,1351,1300,1265,1209,1171,113
5,1100,1067,1034,1002,975,944,917,889,865,839,815,792,772,747,725,705,688,669,650,631,616,599
,584,569,556,540,527,516,499,486,475,462,451,441,426,419,413,402,391,380,374,363,356,348,335,3
28};
char result_file[25],laserwatt[25],wavelength[25],fiberdia[25];
void main()
{
    init();
    resultout();
}
void init()
{
    int j;
    clrscr();
    for(j=0;j<80;j++)
        printf("_");
```

```
printf("\n\n          Conversion Ohm/deg. C.\n\n");
for(j=0;j<80;j++)
    printf("_");
printf("\n\nWrite resultfile\n");
scanf("%s",result_file);
printf("\n\nTime between readings [s]");
scanf("%d",&timestep);
printf("\nLaserwatt ");
scanf("%s",laserwatt);
printf("\nLaser wavelength ");
scanf("%s",wavelength);
printf("\nFiber diameter ");
scanf("%s",fiberdia);
printf("\nLaser shutoff [s] ");
scanf("%d",&laseroff);
printf("\nProbe1 r-coord. [mm]");
scanf("%d",&r1);
printf("\nProbe1 z-coord. [mm]");
scanf("%d",&z1);
printf("\nProbe2 r-coord. [mm]");
scanf("%d",&r2);
printf("\nProbe2 z-coord. [mm]");
scanf("%d",&z2);
}
void resultout()
{
    int timet;
    char label[70];
    FILE *givare;
    givare=fopen(result_file,"w");
    timet=0;
    fprintf(givare,"Laserwatt %s\nWavelength %s\nFiber diameter
%s\n",laserwatt,wavelength,fiberdia);
    fprintf(givare,"Laser shutoff %d s.\n",laseroff);
    fprintf(givare,"Probe1 r= %d mm. z= %d mm.\nProbe2 r= %d
mm. z= %d mm.\n",r1,z1,r2,z2);
    printf("\nAmbiant resistance for probe1\n");
    scanf("%f",&probe1); probe2=0.0;
    conversion();
    fprintf(givare,"Ambiant temperature %3.1f\n",temp1);
    printf("\nPush 1 to correct last pair of registrations\n");
    printf("Push 0 to finish\n\n\n");
```



```

printf("Time\tProbe1\tProbe2\n");
fprintf(givare,"Time\tProbe1\tProbe2\n");
do
{
    printf("%d\t",timet);
    scanf("%f%f",&probe1,&probe2);
    if ((probe1==1)||(probe2==1))
        timet=timet-timestep;
    else
        if (probe1!=0)
            {
                conversion();
                fprintf(givare,"%d\t%3.1f\t%3.1f\n",timet,temp1,temp2);
                timet=timet+timestep;
            }
}
while((probe1!=0)&&(probe2!=0));
printf("\nWrite label of file\n");
scanf("%s",label);
fprintf(givare,"\n%s",label);
fclose(givare);
}

```

```

void conversion()
{

```

```

    int i;
    float x;
    i=0;
    temp1=0.0;
    temp2=0.0;
    if(probe1>3420) temp1=10;
    if(probe1<=332) temp1=100;
    if(probe2>3670) temp2=10;
    if(probe2<=328) temp2=100;
    if(temp1<1)
        {
            while (probe1<=resist1[i])
                i=i+1;
            x=(probe1-resist1[i])/(resist1[i-1]-resist1[i]);
            temp1=11.0+i-x;
        }
    i=0;
    if(temp2<1)

```

```

{
    while (probe2<=resist2[i])
        i=i+1;
    x=(probe2-resist2[i])/(resist2[i-1]-resist2[i]);
    temp2=11.0+i-x;
}

```